ROTORDYNAMICS/DISCHARGE-LINE WATER-HAMMER COUPLING VIA SEALS IN PUMP ROTORDYNAMICS

A Thesis

by

KAIKAI ZHANG

Submitted to the Office of Graduate Studies of
Texas A&M University
in partial fulfillment of the requirements for the degree of

MASTER OF SCIENCE

May 2003

Major Subject: Mechanical Engineering

ROTORDYNAMICS/DISCHARGE-LINE WATER HAMMER COUPLING VIA SEALS IN PUMP ROTORDYNAMICS

A Thesis

by

KAIKAI ZHANG

Submitted to Texas A&M University
in partial fulfillment of the requirements
for the degree of

MASTER OF SCIENCE

Approved as to style and content by:

Dara W. Childs (Chair of Committee)	Luis San Andres (Member)
Jose M. Roesset (Member)	John A. Weese (Head of Department)

May 2003

Major Subject: Mechanical Engineering

ABSTRACT

Rotordynamics/Discharge-line Water Hammer Coupling
Via Seals in Pump Rotordynamics. (May 2003)
Kaikai Zhang,
B.S., Peking University
Chair of Advisory Committee: Dr. Dara W. Childs

A new closed-loop frequency-domain model is developed to incorporate the water hammer effect with pump rotordynamics, in order to investigate the sub-synchronous instability problem observed in a field pump. Seal flow-rate perturbations due to eccentricity are calculated from Soulas and San Andres's seal code. A complete transfer function matrix between rotor motion and reaction force due to pressure perturbation is developed in detail. Stability analysis with transfer-function 'add-in' modules is conducted in XLTRC^2. Seal clearances and the reaction force angle are found to be important in shifting natural frequencies and damping. The sub-synchronous instability observed in the field is duplicated successfully with double-clearance seals.

ACKNOWLEDGMENTS

I am deeply grateful to my supervisor Dr. Dara Childs. His financial support made this work possible. He guided me from the start and gave me lots of ideas, suggestions and encouragement. His rich knowledge in the field of turbomachinery rotordynamics and insight into the problem made this job a lot easier for me. I benefitted a great deal from my discussions with Dr. Childs. The years I spent at Texas A&M University may become the treasure of my whole life. I particularly appreciate Dr. San Andres for his permission to use the seal code, and also for his careful review of the draft, and all his helpful advice and corrections. I am very pleased to thank Avijit and Luis for their kind help in using XLTRC^2. It is my pleasure to acknowledge the assistance I received from Arthur in preparing the final exam and correcting the thesis. My thanks are also extended to Jon and Bugra in the Turbomachinery Laboratory, who shared good times with me in the lab.

I am always grateful to my parents. Without their solid support, I would not have gotten to this point at all. I would dedicate this thesis to my girlfriend, Wang Tingting, for her love.

TABLE OF CONTENTS

Page

Page

LIST OF FIGURES

Page

Page

Page

NOMENCLATURE

$\delta\dot{X}_{seal}$	planar rotor motion at seal [L/T]
$\delta\dot{q}_{seal}$	seal flow-rate perturbation at impeller seal inlet [L^3/T]
$\delta\dot{Q}_{pump}$	perturbation of the exit flow-rate of the pump [L^3/T]
δP_{pump}	pump discharge pressure perturbation [F/L^2]
$\delta f_{impeller}$	the reaction force [F]
$\Re$	attenuation factor in Corley's model
τ_d	time delay in Corley's model [T]
β	reaction force angle
R_d	resistance [FT/L^5]
c	velocity of propagation of the pressure wave [L/T]
u	velocity of the fluid [L/T]
P	pressure [F/L^2]
X, Y, Z	rotor motion coordinate system
x, y, z	seal-eccentricity-oriented coordinate system
R_x, R_y	components of rotor position vector in x, y, z system[L]
R_X, R_Y	components of rotor position vector in X, Y, Z system [L]
$Z_{qx}(s), Z_{qy}(s)$	transfer functions between rotor motion and seal flow-rate perturbation (perturbed seal flow-rate per unit motion) [L^2/T]

α_i	angle between X axis and x axis
e_0	the static eccentricity
e_{0X}, e_{0Y}	components of static eccentricity
$\delta\dot{q}_x, \delta\dot{q}_y$	the global seal flow-rate perturbation in x and y direction [L^3/T]
$\delta\dot{q}_{xr}, \delta\dot{q}_{xi}$	real part and imaginary part of $\delta\dot{q}_x$ [L^3/T]
$\delta\dot{q}_{yr}, \delta\dot{q}_{yi}$	real part and imaginary part of $\delta\dot{q}_y$ [L^3/T]
Ω	excitation frequency [$1/T$]
ω	running speed [$1/T$]
s	Laplace transform operator [$1/T$]
j	$\sqrt{-1}$
A_{imp}	the projected area of the discharge impeller [L^2]
$T(s)$	transfer function between seal flow-rate perturbation and discharge pressure perturbation [FT/L^5]
$G_{11}, G_{12}, G_{21,} G_{22}$	components of the complete transfer function matrix [F/L]

I. INTRODUCTION

Corley [1] cites a case study involving large water injection pumps. After about one year of operation, some of the pumps became unstable at a frequency near the pump's first natural frequency. Someone noted that only pumps with an abrupt decrease in diameter at the pump inlet and increase at pump discharge had the problem, while pumps with a gradual decrease or increase in diameter did not. The instability was eliminated in one of the pumps by replacing the abrupt piping expansion transition with a gradual piping expansion transition at pump discharge and a gradual contraction transition at pump inlet. Corley [2] subsequently developed a model to explain the initial instability and its resolution. He implemented a feed-back loop model between planar rotor motion at a seal $\delta\dot{X}_{seal}$ and a reaction force developed by a flow perturbation at the discharge. His feed-back model involves the following procedures:

1. Perturbed motion of the rotor $\delta\dot{X}_{seal}$ at a seal location next to the exit impeller causes a leakage perturbation at the impeller seal inlet $\delta\dot{q}_{seal}$, yielding the same perturbation of the exit flow of the pump; i.e., $\delta\dot{Q}_{pump} = \delta\dot{q}_{seal}$.

2. $\delta\dot{Q}_{pump}$ causes a perturbation in the pump discharge pressure δP_{pump} defined by a perturbation of the pump's H-Q curve.

This thesis follows the format of ASME Journal of Tribology.

3. Inserting $\delta P_{pump}(t)$ into the discharge line of the pump causes a negative, delayed, and attenuated pressure wave $\delta P_{pipe}(t+\tau_d) = -\Re \times \delta P_{pump}(t)$, with the attenuation factor $\Re < 1$. This model implies that a positive step-function pressure perturbation into the discharge line would produce (after a time delay τ_d) a negative step-function reflected wave at reduced amplitude. Corley obtained the attenuation factor $\Re$ from an acoustics analysis.

4. The reflected wave δP_{pipe} acts on the projected area of the impeller to produce the reaction force $\delta f_{impeller} = -\delta P_{pipe} \times A_{imp}$, that closes the loop between rotor motion $\delta \dot{X}_{seal}$ and the reaction force $\delta f_{impeller}$, which may either be stabilizing or leading to more displacement in the seal, depending on the time delay and rotor speed.

Corley used a digital computer code that simulates an analog computer to perform repeated transient analyses on his model. He showed that an instability could be produced by varying the time delay τ_d . Also, the rotor natural frequency could be varied from around 65HZ to 50HZ by varying the time delay. Hence Corley simultaneously identifies an instability mechanism and shows how the rotor natural frequency can be shifted due to an interaction with the discharge line.

Corley's transient modeling approach cannot be used for conventional stability analysis since it requires multiple time simulations to map out the stability characteristics. Moreover, his time-delay acoustic model specifies two different pressures at one location as above procedure 3 shows, which is an evident deficiency. Corley's planar model is

incompatible with most current rotordynamic models, which describe rotor motion in two planes. In this thesis, a direct frequency-domain model is developed to replace Corley's transient modeling approach for stability analysis. The pipeline dynamics is modeled via finite element method using a tapered flow element. Soulas and San Andres' [3] eccentric-seal flow computational solution is used for the seal flow-perturbation versus rotor-motion transfer function. The complete rotor-motion/reaction-force transfer function is developed as a 'plug in' transfer function module into XLTRC^2 (a rotordynamics code developed by Turbomachinery Laboratory). The resultant closed-loop transfer-function model is running with different seal clearances and discharge pipe configurations, to investigate the stability characteristics. Comparisons with test results were conducted to evaluate the new model.

II. RESEARCH OBJECTIVES

The research carried out here answers the following questions:

1. How does seal eccentricity influence rotordynamic characteristics?

2. How does seal clearance influence the rotordynamic characteristics?

3. How do the rotordynamic characteristics change with pipe configurations?

4. How does the reaction-force angle β affect the rotordynamic characteristics?

5. How does the running speed affect the rotordynamic characteristics?

6. Can the Water-Hammer/Rotordynamics Coupling model simulate correctly the field results?

III. ROTOR MODEL IN XLTRC[2]

1. Pump design

The water injection shipper pump (Figure 1) is a large, two-stage, double-suction volute pump. The shipper and booster pumps are directly driven by a two-shaft combustion gas turbine. The $16\times16\times20DVMF$ pump has a conventional pressure dam and babbitted sleeve bearing to suppress oil whirl at the higher speeds. Wear rings for the pump are of conventional design with a stellite overlay and clearances of 0.53 to 0.635 mm (0.021 to 0.025 in.). Gear-type couplings were used on the train. The original pump had a discharge transition from 0.406m (16 in) to 0.609 m (24 in) over a span of 0.51 m (20 in).

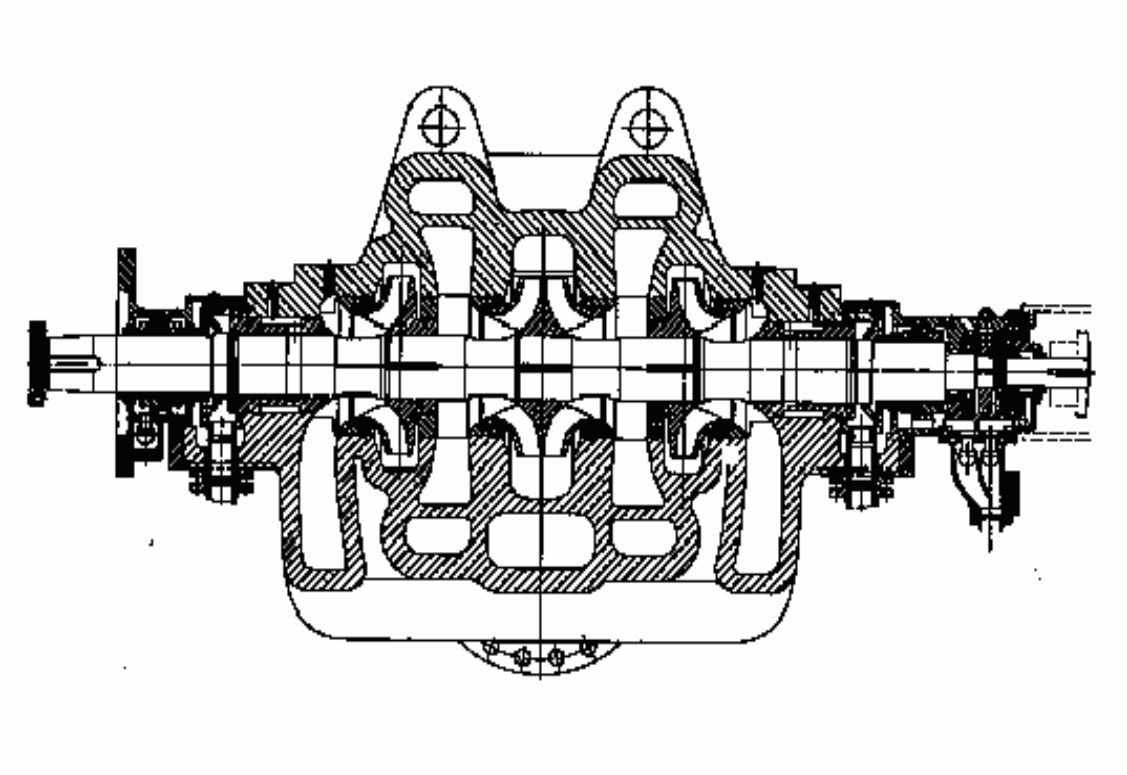

Figure 1 Outline Drawing of the 16*16*20 DVMF Shipping Pump

2. Rotor model

Figure 2 shows the rotor model in XLTRC^2, which is based on the finite element method. Half the mass of the couplings is added at each end of the pump. Seals and pressure dam bearings coefficients were calculated from the built-in programs of XLTRC^2 and added to the model. The impeller's influence was also taken into account by adding support files, whose coefficients were calculated as described by Childs [4].

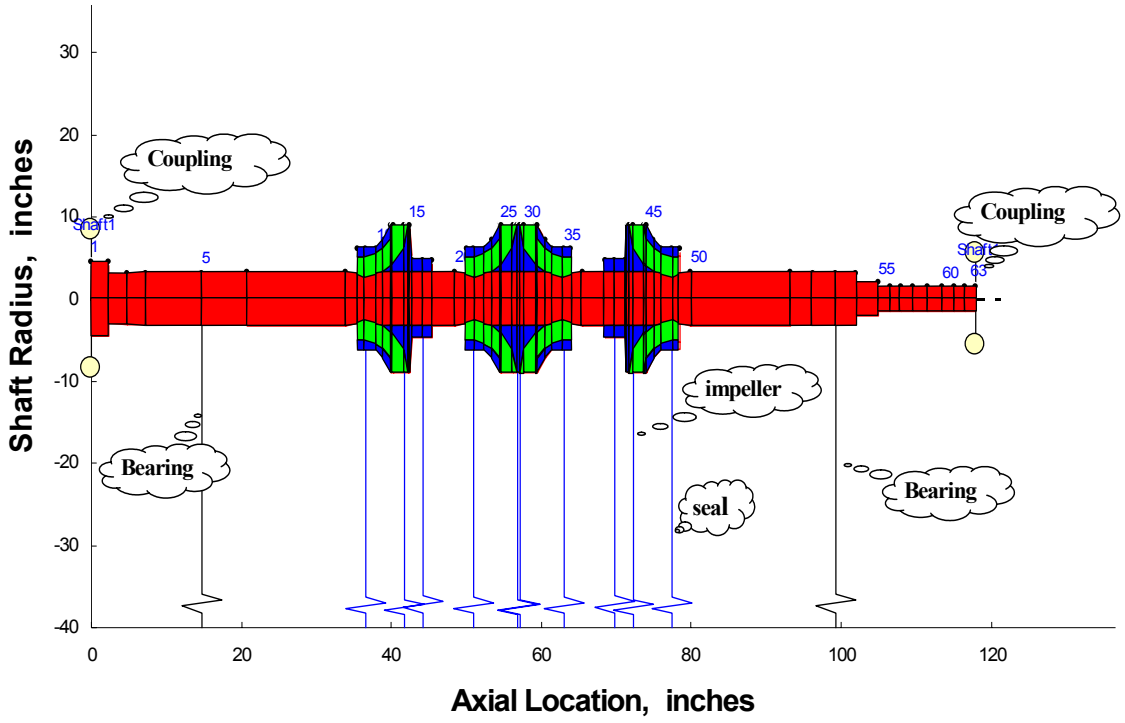

Figure 2 Rotor Model in XLTRC^2

The rotor has a total length of 3 meters (118 in) and mass of 840 kg (1852 lbm), including the couplings. Figure 3 to Figure 6 show the first four damped mode shapes with the original-clearance 0.635mm (0.025 in) seal. Note that the first two modes are bounce

and pitch modes, which are rigid-body modes. The third one is backward whirling. The fourth one is sinusoidal, with low amplitude at the bearing locations, and maximum amplitude at the seal locations.

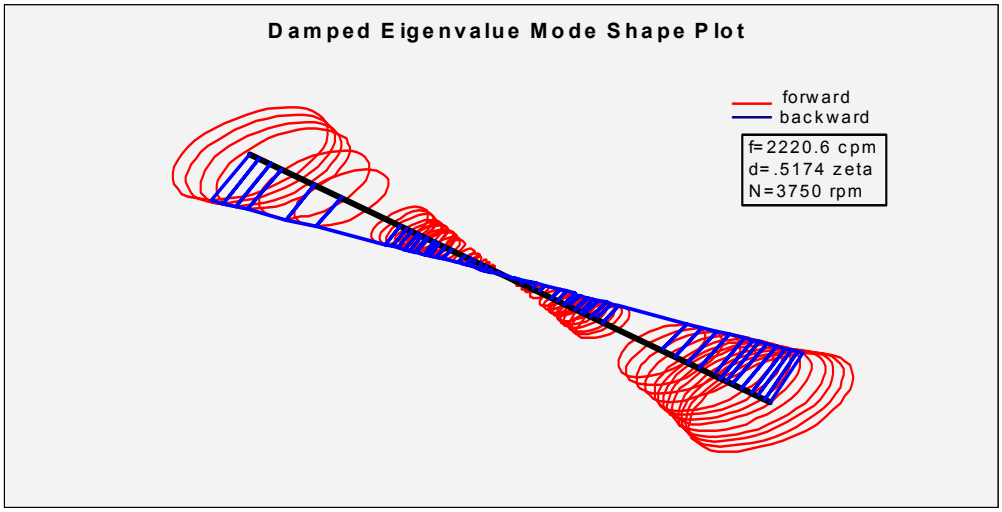

Figure 3 First Damped Mode Shape with Original-clearance Seal

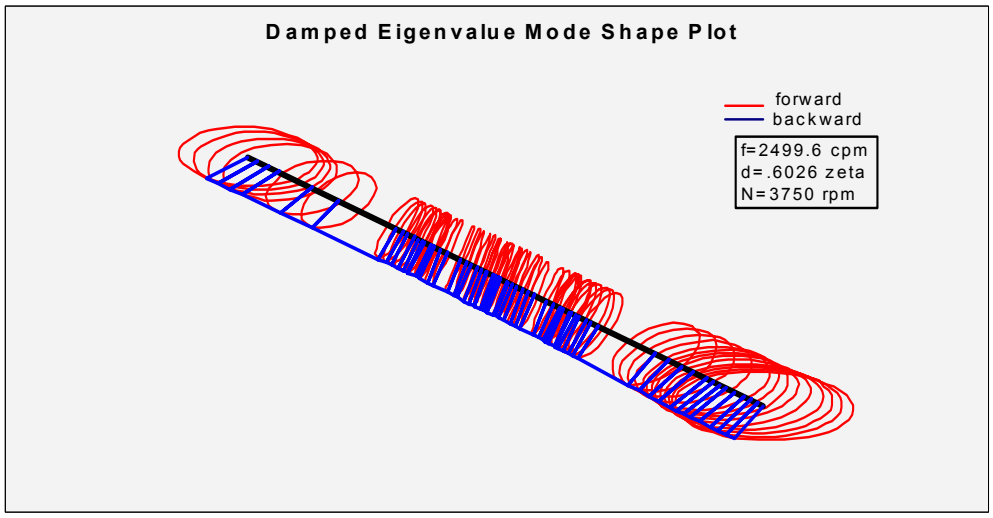

Figure 4 Second Damped Mode Shape with Original-clearance Seal

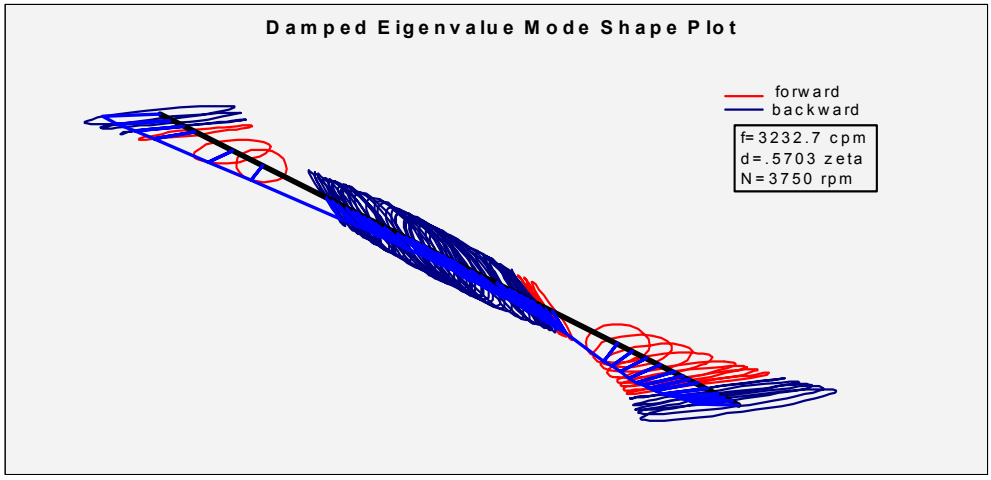

Figure 5 Third Damped Mode Shape with Original-clearance Seal

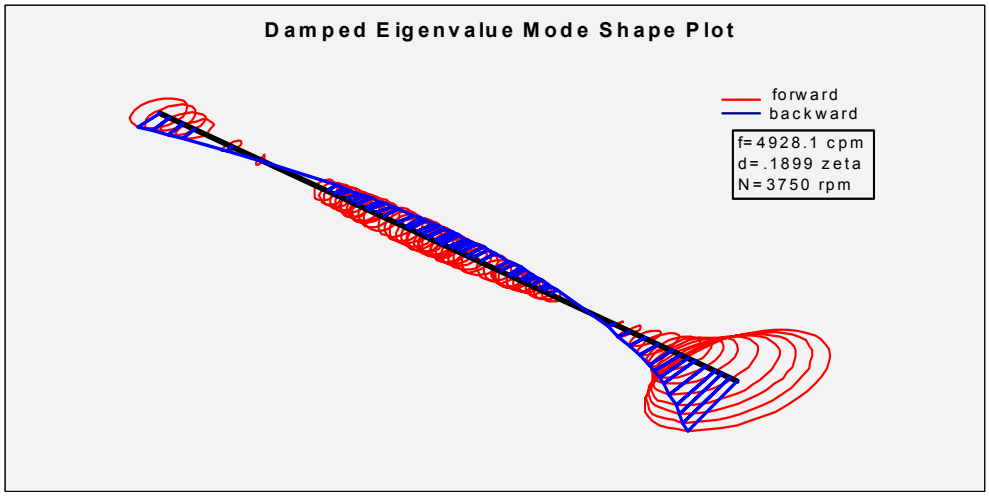

Figure 6 Fourth Damped Mode Shape with Original-clearance Seal

With the original-clearance seal 0.635 mm (0.025 in), the rotor has a damped critical speed at 3150 RPM, while with double-clearance seal 1.27 mm (0.05 in), it decreases to 2900 RPM. Also, the damping ratio decreases. No instability problem was predicted in either case from the rotordynamic root locus plots. Figure 7 to Figure 10 show the damped critical speed maps and rotordynamic root locus plots with original-clearance and double-

clearance seals respectively. All these frequency components are well damped except the one just above 6000 CPM. Normally, rotor system with double-clearance seal will give lower natural frequencies and damping ratio. However, for those frequency components associated with a mode that has a vibration node in the middle of the rotor, double-clearance seal shows no observable influence.

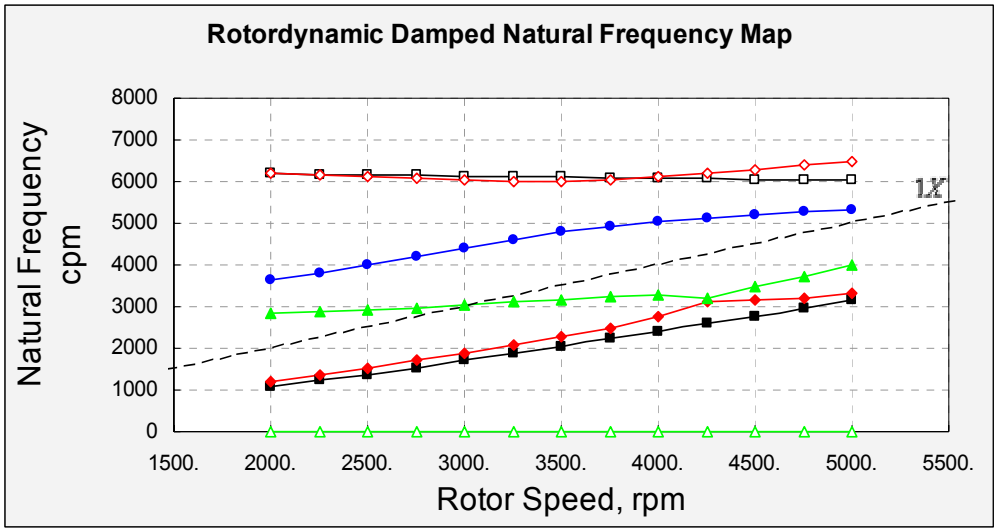

Figure 7 Rotordynamic Damped Natural Frequency Map with Original-clearance Seal 0.635mm (0.025 in)

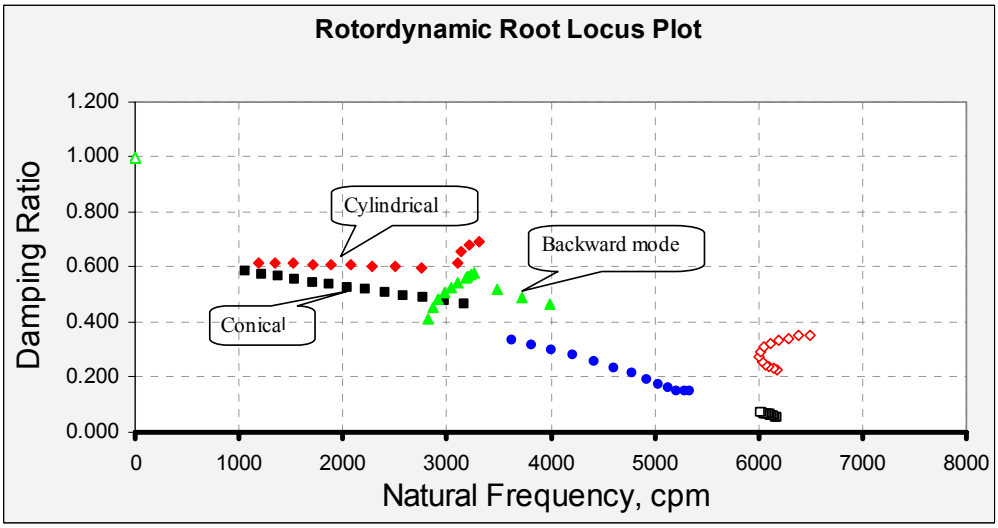

Figure 8 Rotordynamic Root Locus Plot with Original-clearance Seal 0.635mm (0.025 in)

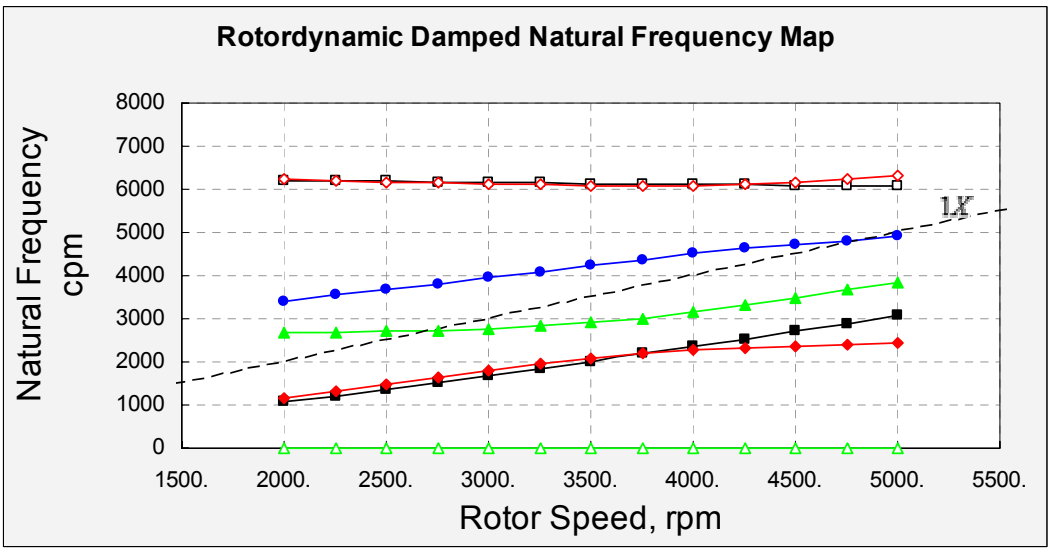

Figure 9 Rotordynamic Damped Natural Frequency Map with Double-clearance Seal 1.27mm (0.05 in)

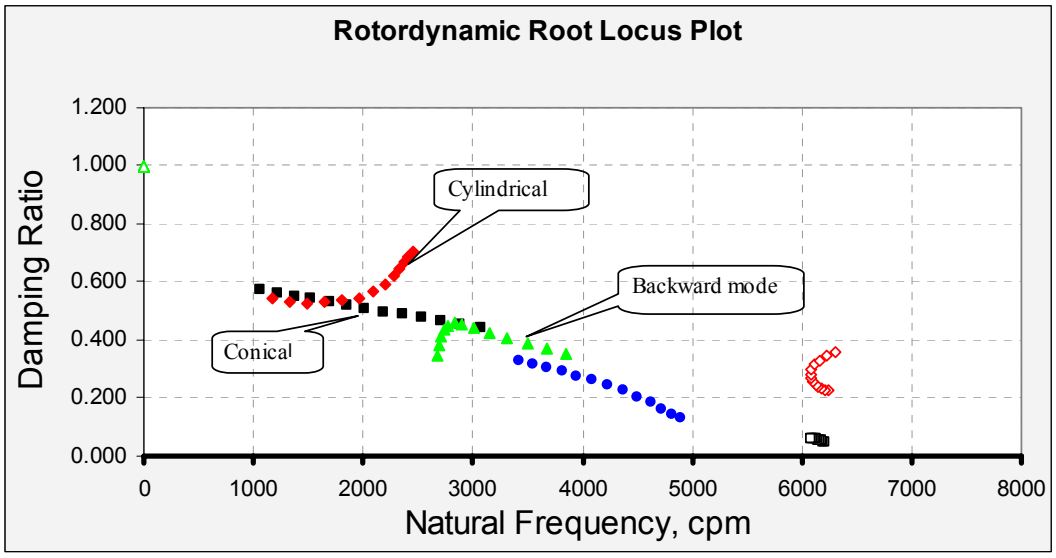

Figure 10 Rotordynamic Root Locus Plot with Double-clearance Seal 1.27mm (0.05 in)

IV. CLOSED LOOP MODEL

1. Standard water-hammer analysis for pipeline

The simple water-hammer example of Figure 11 consists of an inlet line connecting a tank to a pump that provides flow to a discharge line, which ends at a valve with resistance R_d.

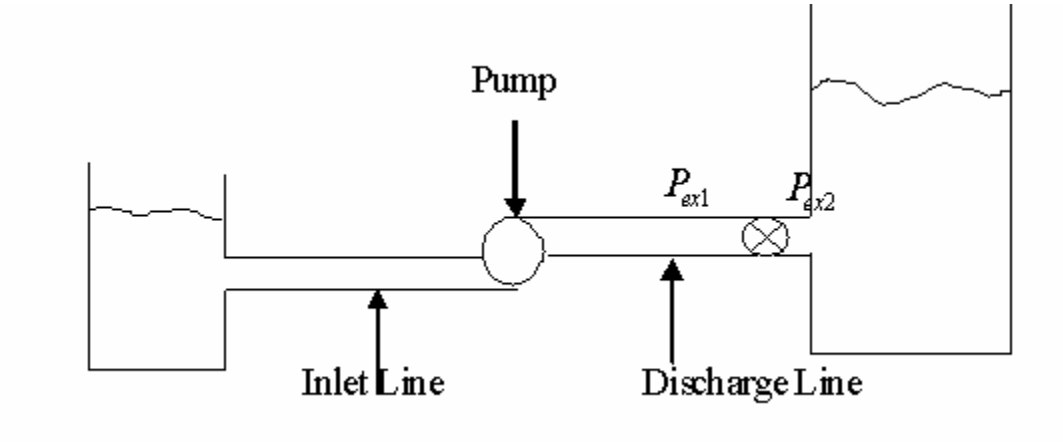

Figure 11 Water-hammer Example of Pump

Figure 12 shows a typical perturbed flow-rate and pressure model, where the exit perturbed flow from the inlet line is denoted $\delta\dot{q}_{pump}$, the pressure perturbation at the pump inlet and exit are denoted $\delta P_{inlet}, \delta P_{discharge}$, $\overline{A}$ is a damping source that resulted from the pump's H-Q curve, which models the pressure difference across the pump. δP_{ex1} denotes the pressure perturbation just upstream of the valve and $\delta\dot{q}_{ex}$ denotes the perturbed flow-rate at the valve.

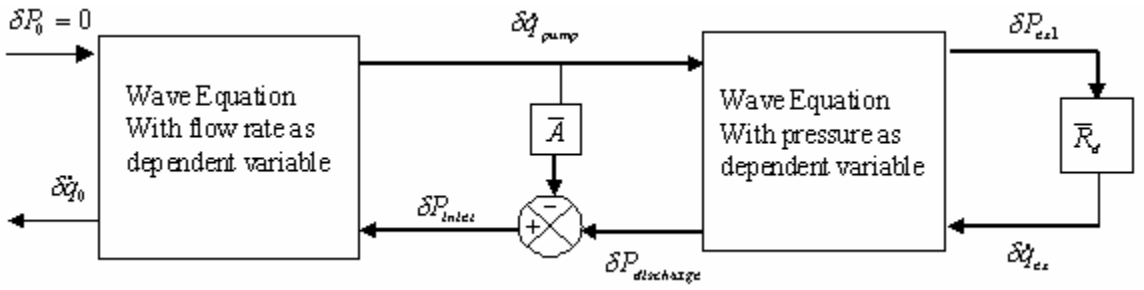

Figure 12 Perturbed Water-hammer Flow-rate and Pressure Model

This model can be used to consider flow and pressure perturbations in the system due to disturbances in the system, e.g., a perturbation in the discharge valve position. The wave-equation model for the inlet and discharge lines is normally converted into a system of ordinary differential equations that can be developed via finite-element analysis.

2. Finite element development for pipeline

Y. Rocard [5] gives the wave equations governing the propagation of plane waves in horns. Either equation (1) or equation (2) can be used to account for the expansions or contractions in the discharge lines or inlet lines.

$$c^2\left[\frac{\partial^2 u}{\partial z^2}+\frac{2}{z}\frac{\partial u}{\partial z}-2\frac{u}{z}\right]=\frac{\partial^2 u}{\partial t^2} \tag{1}$$

$$c^2\left[\frac{\partial^2 P}{\partial z^2}+\frac{2}{z}\frac{\partial P}{\partial z}\right]=\frac{\partial^2 P}{\partial t^2} \tag{2}$$

Where u is velocity of the fluid along the pipe, P is the pressure, and c is the velocity sound. Equation (1) is used for inlet line where velocity is the desired variable; Equation (2)

is used for discharge line where pressure is the desired variable. Laplace transformation [6] are taken to obtain the transfer functions. Appendix A shows the full development of the transfer functions between seal flow-rate perturbation and perturbed pressure.

3. Seal flow-rate perturbation calculation

Soulas and San Andres [3] gives the definitions of the perturbed axial flow-rate and the global perturbed axial flow-rate, which is given as an integral of the perturbed axial flow-rate over the circumference. They also present the results obtained for the determination of the global perturbed axial flow-rate at the synchrounous frequency as a function of the seal static dimensionless eccentricity at the inlet and exit planes of the seals tested by Marquette[7]. Similar calculations were conducted for the eye seals of the discharge impeller. Each seal has diameter 314.3 mm (12.375 in), axial length 63.5 mm (2.5 in). Appendix C gives the input data for seal flow-rate perturbation calculation. For both the original-clearance seals and double-clearance seals, 0.1 static eccentricity (the static dimensionless eccentricity was taken from the static load deflection calculation in XLTRC^2. This analysis calculates the rotor deflection at certain running speed with bearing coefficients only. The results at seal location are taken for seal flow-rate perturbation calculation.) was used. The global flow-rate perturbation due to general motion is:

$$\delta\dot{q}_{seal}(s) = Z_{qx}(s)\cdot R_x(s) + Z_{qy}(s)\cdot R_y(s) \tag{3}$$

Where R_x, R_y are components of the rotor position vector that are parallel and perpendicular respectively, to the static eccentricity vector e_0 ; $Z_{qx}(s), Z_{qy}(s)$ are transfer functions between rotor motion and seal flow-rate perturbation parallel and perpendicular to the static eccentricity vector respectively. Since the flow-rate perturbation calculations are performed by using another coordinate system X, Y, Z , where Z is along the rotor axis and Y vertical, a coordinate transformation between X, Y, Z and x, y, z is necessary here. Figure 13 shows the stationary system X, Y, Z and seal eccentricity-oriented system x, y, z . The x axis of the x, y, z system is directed along e_0 ; hence, α_i , the angle between the x and X is:

$$\alpha_i = \tan^{-1}\left(\frac{e_{0Y}}{e_{0X}}\right) \tag{4}$$

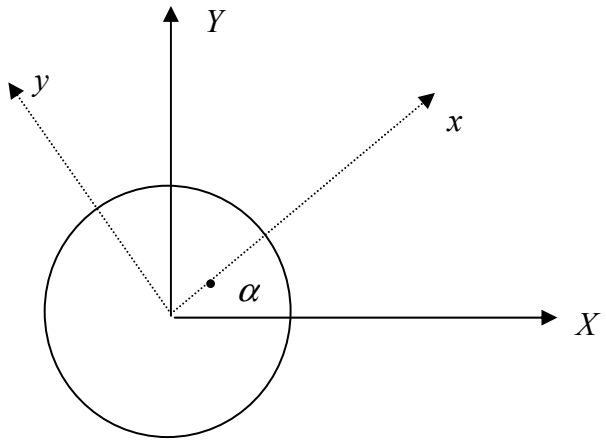

Figure 13 Coordinate Systems

In this model, α_i is also taken from the static load deflection results in XLTRC[2]. The components of the seal displacement vector in the x, y (seal-eccentricity-oriented) coordinate system are:

$$R_{ix} = R_{iX}\cos(\alpha_i) + R_{iY}\sin(\alpha_i),\ R_{iy} = -R_{iX}\sin(\alpha_i) + R_{iY}\cos(\alpha_i) \tag{5}$$

From equation (3), the perturbed flow-rate due to motion within a seal at Z_i is:

$$\begin{aligned}\delta\dot{q}(s) &= Z_{qx}(s)[R_{iX}(s)\cos(\alpha_i) + R_{iY}(s)\sin(\alpha_i)] + Z_{qy}(s)[-R_{iX}(s)\sin(\alpha_i) + R_{iY}(s)\cos(\alpha_i)] \\ &= R_{iX}(s)[Z_{qx}(s)\cos(\alpha_i) - Z_{qy}(s)\sin(\alpha_i)] + R_{iY}(s)[Z_{qx}(s)\sin(\alpha_i) + Z_{qy}(s)\cos(\alpha_i)]\end{aligned} \tag{6}$$

Figure 14 and Figure 15 show the calculated results of $Z_{qx}(s), Z_{qy}(s)$ versus excitation frequency at the running speed 4700 RPM, with original-clearance 0.635 mm (0.025 in) and double-clearance 1.27 mm (0.05 in) seals respectively. The calculated results of $Z_{qx}(s), Z_{qy}(s)$ versus excitation frequency at the running speed 3750 RPM are also shown as Figure 16 and Figure 17, with original-clearance 0.635 mm (0.025 in) and double-clearance 1.27 mm (0.05 in) seals respectively. Four different series shown in these figures represent real part and imginary part of $Z_{qx}(s), Z_{qy}(s)$, as labels show. Notice that the real part of Z_{qx} (or $\frac{\delta\dot{q}_{xr}}{R_x}$) is slightly increasing with changing frequency, while the imaginary part of Z_{qx} (or $\frac{\delta\dot{q}_{xi}}{R_x}$) increases linearly with increasing frequency. A transfer function between motion in the x direction and the flow perturbation model can be modeled as:

$$\frac{\delta \dot{q}_x}{R_x} = a_0 + a_1 j\Omega = a_0 + a_1 \cdot s = Z_{qx}(s) \tag{7}$$

The results for $\delta \dot{q}_{yr}$, $\delta \dot{q}_{yi}$ (real part and imginary part of $\delta \dot{q}_y$) are more complicated. The real part of Z_{qy} (or $\frac{\delta \dot{q}_{yr}}{R_x}$) increases in a more or less quadratic manner with increasing frequency. It reaches a minimum value at 4300 RPM and then begins to increase. The imaginary part of Z_{qy} (or $\frac{\delta \dot{q}_{yi}}{R_x}$) increases linearly with excitation frequency. Notice that the real part of Z_{qy} is much smaller than the other flow perturbation terms and close to zero. For simplicity, a reasonable transfer function between motion in the y direction and the flow perturbation can be modeled as:

$$\frac{\delta \dot{q}_y}{R_y} = b_1 j\Omega = b_1 \cdot s = Z_{qy}(s) \tag{8}$$

Also, note that the perturbed flow-rate with double-clearance seal has much higher $\frac{\delta \dot{q}_{xi}}{R_x}$ (about three times) than that of original-clearance seal, which is found later to play an important role in making the pump rotordynamic system unstable.

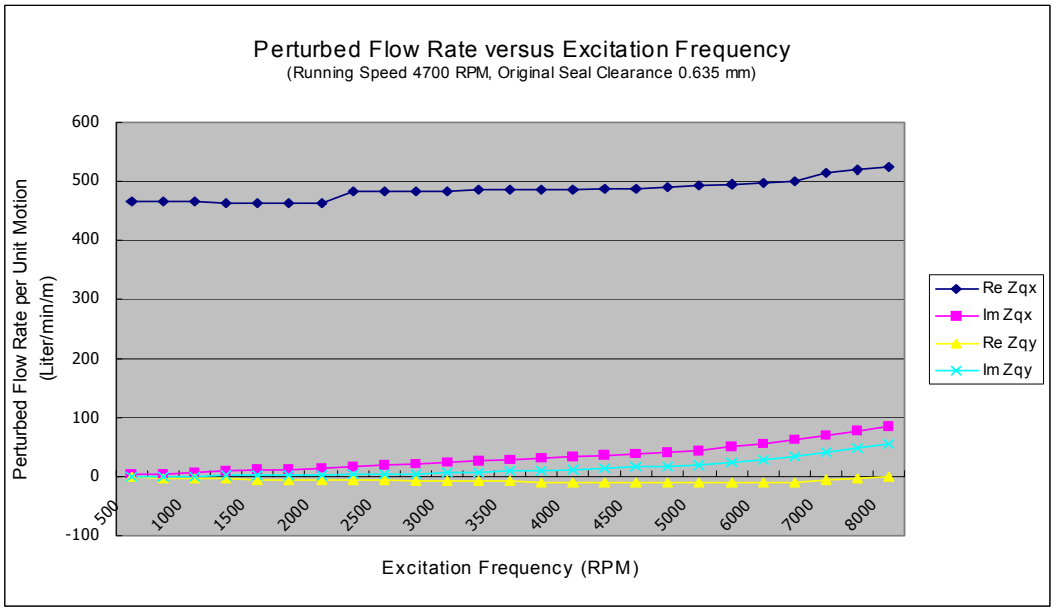

Figure 14 Perturbed Seal Flow-rate per Unit Motion Versus Excitation Frequency with Original-clearance Seal at Running Speed of 4700 RPM

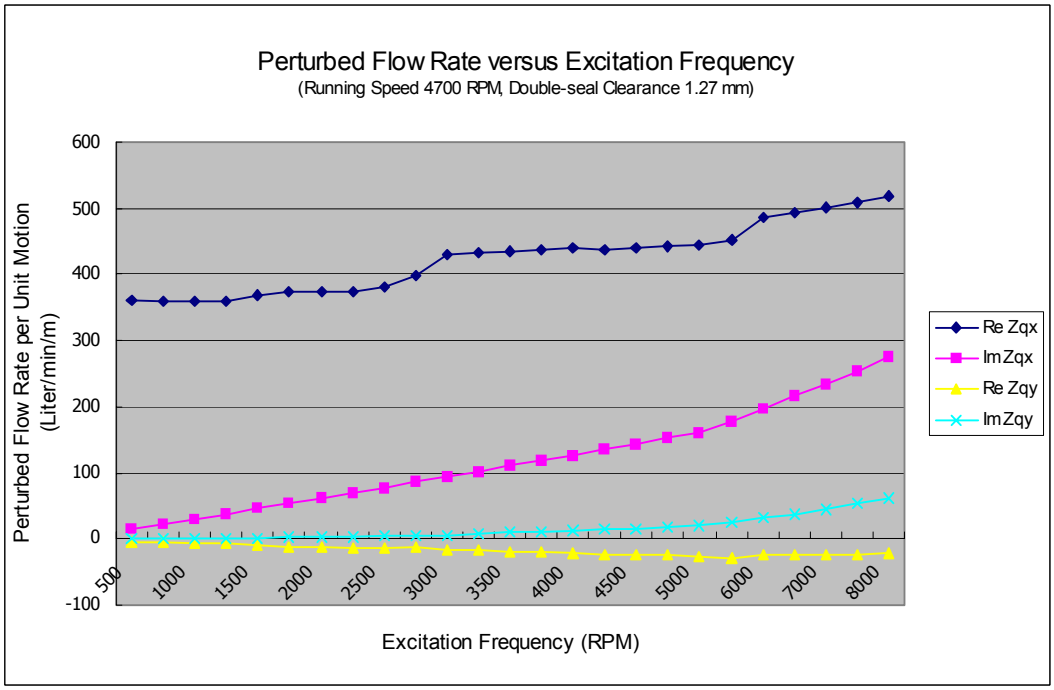

Figure 15 Perturbed Seal Flow-rate per Unit Motion Versus Excitation Frequency with Double-clearance Seal at the Running Speed of 4700 RPM

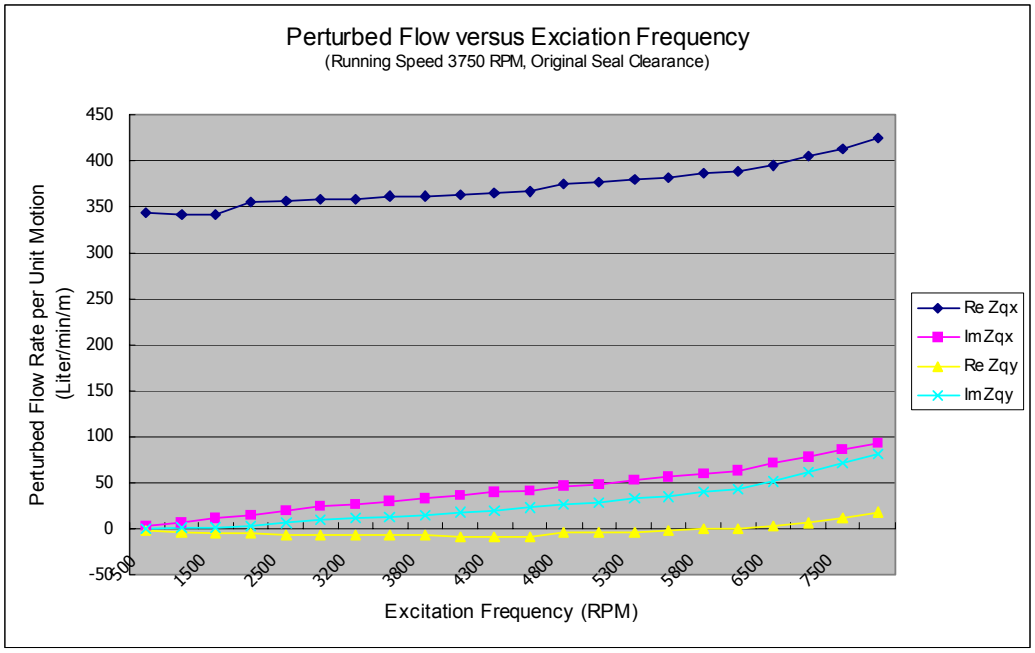

Figure 16 Perturbed Seal Flow-rate per Unit Motion Versus Excitation Frequency with Original-clearance Seal at the Running Speed of 3750 RPM

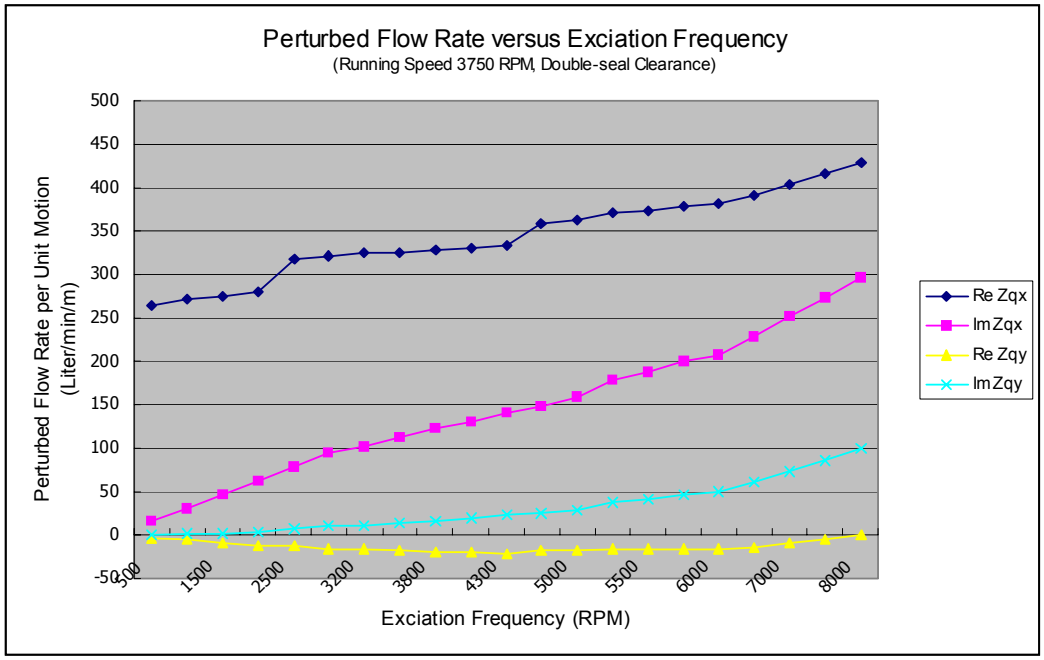

Figure 17 Perturbed Seal Flow-rate per Unit Motion Versus Excitation Frequency with Double-clearance Seal at the Running Speed of 3750 RPM

4. Coupling of rotor motion to water-hammer dynamics

Equation 6 defines the perturbed flow-rate that is produced at an eccentric seal due to rotor motion. The question is: How does the perturbed flow in the seal influence the unsteady motion in the inlet or discharge lines? Perturbed motion at the wearing-ring seal for the first stage of a pump would produce perturbed flow at its exit that would then directly perturb the inlet flow of the pump. This sort of pressure oscillation at the pump inlet would probably create an axial oscillation of the pump rotor versus a radial rotor perturbation. Perturbed motion of a wearing-ring or inter-stage seal at an interior impeller would not as directly influence the flow at either the inlet or discharge flow of the pump. For both straight-through and back-to-back pumps, perturbed flow from the inlet of the balance-piston seal will directly perturb the exit flow of the pump; hence, for this discussion, only the simpler question will be considered: How does perturbed motion at the exit balance-piston seal influence unsteady flow in the discharge line? Figure 18 illustrates the perturbed flow-rate from the seal $\delta\dot{q}_{seal}$ being added to the perturbed pump flow-rate $\delta\dot{q}_{pump}$. The net perturbed flow $\delta\dot{q}_{discharge}$ is injected into the discharge-line and produces (eventually) a perturbed pressure disturbance at the pump discharge.

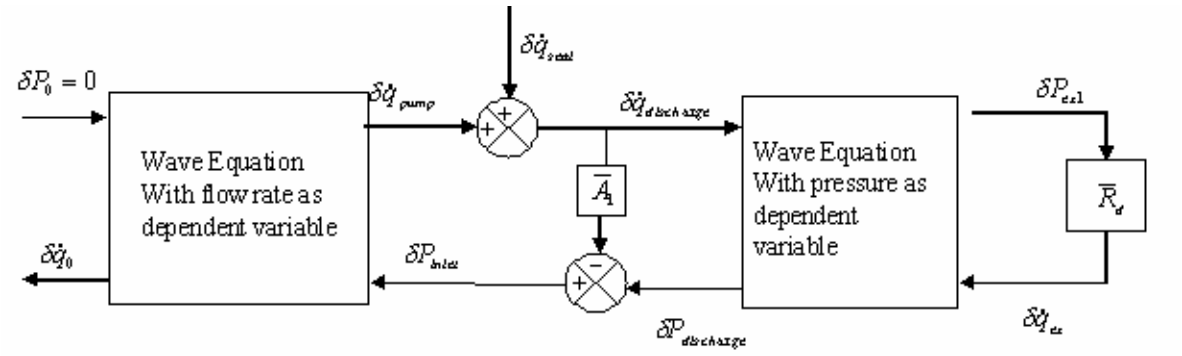

Figure 18 Perturbed Water-hammer Flow-rate and Pressure Model with Perturbed Flow-rate Injection $\delta \dot{q}_{seal}$ from a Seal

5. Coupling of pressure oscillations to rotor motion

The perturbed pressure oscillation at the pump discharge acts on projected area of the discharge impeller and closes the loop on the model. Figure 19 shows the discharge pipe of a volute parallel to the X axis. The force acting on the rotor due to a pressure perturbation on the rotor is oriented with respect to the $-Y$ axis by the reaction force angle β. This angle should reasonably range from -90 to 90 degrees. More precisely, it is probably close to 0 degree in this case. The resultant force on the discharge impeller is $\delta P_{discharge} A_{im}$, where A_{imp} is the projected area of the discharge impeller. Its vector definition is:

$$\begin{bmatrix} \delta f_{iX} \\ \delta f_{iY} \end{bmatrix} = \delta P_{discharge} A_{im} \begin{bmatrix} -\sin\beta \\ \cos\beta \end{bmatrix} \tag{9}$$

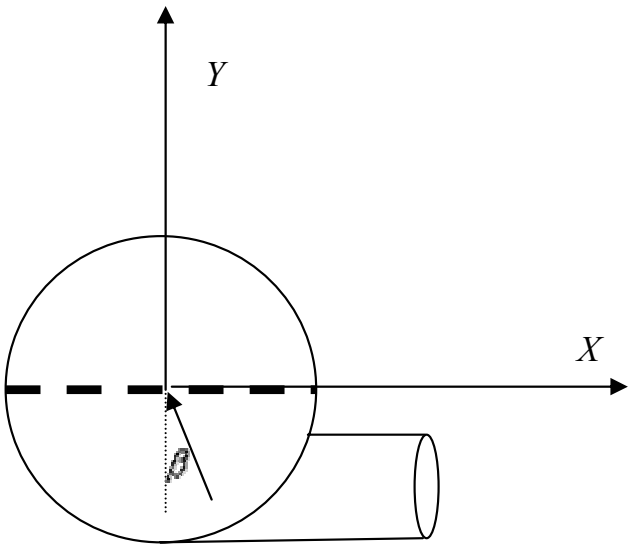

Figure 19 Pump Volute Discharge

6. Complete closed-loop model

Figure 20 shows the complete closed-loop model. Starting with the rotordynamic model, a perturbation in the rotor's position at the balance-piston seal location (R_{iX}, R_{iY}) causes a perturbation in the flow-rate at the inlet to a seal $\delta\dot{q}_{seal}(s)$. This flow perturbation at the inlet to the pump discharge line causes a change in the pump discharge pressure $\delta P_{discharge}$. This perturbation, $\delta P_{discharge}$, acts on the projected area of the impeller and develops the reaction force components $(\delta f_{iX}, \delta f_{iY})$. For this double-suction discharge impeller, $\delta\dot{q}_{seal}(s)$ is doubled as a single perturbation for convenience, which is reasonable since the two seals are pretty close to each other.

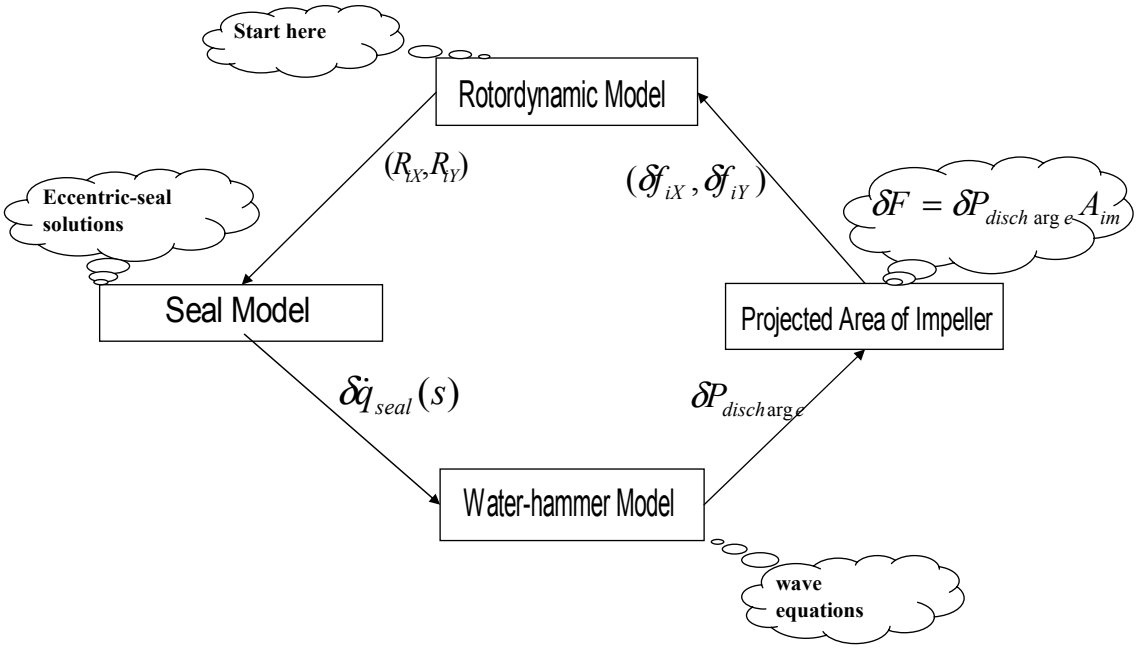

Figure 20 Complete Closed-loop System

Streeter and Wylie [8] show how to calculate the infinite termination impedance Z_C, which is used to simulate the effect of the long shipping pipe. Figure 21 shows the complete transfer function between rotor displacement (R_{iX}, R_{iY}) and the reaction force components $(\delta f_{iX}, \delta f_{iY})$, as a 2×2 transfer-function matrix.

$$\begin{bmatrix} \delta f_{iX} \\ \delta f_{iY} \end{bmatrix} = \delta P_{discharge} A_{im} \begin{bmatrix} \sin\beta \\ -\cos\beta \end{bmatrix} = \delta \dot{q}(s) T(s) A_{impeller} \begin{bmatrix} \sin\beta \\ -\cos\beta \end{bmatrix} = \begin{bmatrix} G_{11}(s) & G_{12}(s) \\ G_{21}(s) & G_{22}(s) \end{bmatrix} \begin{bmatrix} R_{iX} \\ R_{iY} \end{bmatrix} \tag{10}$$

Where:

$$
\begin{aligned}
G_{11}(s) &= [Z_{qx}\cos(\alpha_i) - Z_{qy}\sin(\alpha_i)]T(s)A_{impeller}\sin\beta \\
G_{12}(s) &= [Z_{qx}\sin(\alpha_i) + Z_{qy}\cos(\alpha_i)]T(s)A_{impeller}\sin\beta \\
G_{21}(s) &= -[Z_{qx}\cos(\alpha_i) - Z_{qy}\sin(\alpha_i)]T(s)A_{impeller}\cos\beta \\
G_{22}(s) &= -[Z_{qx}\sin(\alpha_i) + Z_{qy}\cos(\alpha_i)]T(s)A_{impeller}\cos\beta
\end{aligned}
\tag{11}
$$

$T(s)$ is the transfer function calculated for the pipeline as discussed in Appendix B. The projected area of the impeller is estimated to be $0.08395\,m^2$ ($130\,in^2$). The complete transfer function might have the same order ($4\cdot N+1$) in the numerator and the denominator, which depends on the number of modes (N) taken into account in the water-hammer model. Kleynhans and Childs [9] and Appendix D show how to develop a state-variable model and calculate the complex eigenvalue with general numerator-denominator form transfer functions.

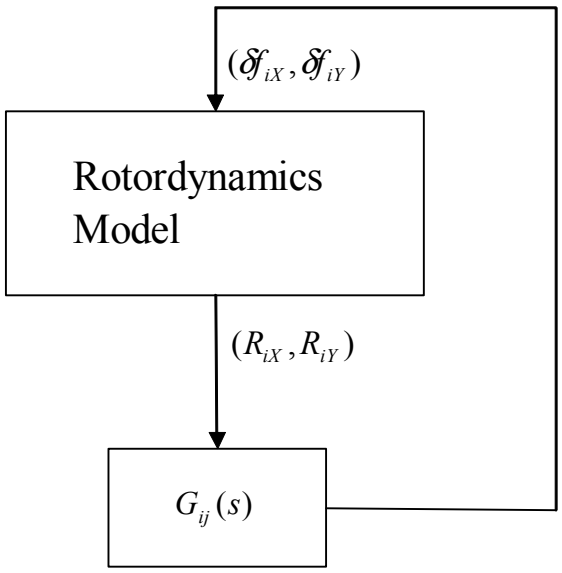

Figure 21 Closed-loop Model Showing the Transfer Function between the Rotor Displacement Vector and the Reaction Forces

V. MODEL RESULTS AND DISCUSSION

The closed-loop model results are presented in this section. Only the discharge line is considered here, since the model including the inlet-line had minimal influence on the results. The original-clearance seal of 0.635mm (0.025inch) and double-clearance seal of 1.27mm (0.05inch) are used to investigate the effects of seal clearance. The reaction-force angle β is also varied to study its effects on rotordynamic stability. Different discharge pipe configurations are examined to investigate the influence on rotordynamic characteristics. Figure 22 shows two discharge pipes used in the model. The original discharge transition has left diameter of 0.406m (16 in) and right diameter of 0.609 (24 in), over a span of 0.51 m (20 in). The modified gradual expansion discharge transition has the same left diameter and right diameter, over a longer span of 1.83 m (72 in). Different running speeds are examined to show how the rotordynamic characteristics change with running speeds.

The feed-back reaction force angle (β) was found to have significant influence on rotordynamic characteristics. Figure 23 to Figure 27 show the rotordynamic root locus plot with different seal clearances, discharge pipe configurations and running speeds, where the reaction force angle (β) varies from -90 to 90 degrees. Figure 25 shows the first four damped modes with water-hammer coupling, double-clearance seal and $\beta = 15^{\circ}$.

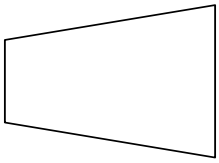

Original discharge pipe: LD=0.406m, RD=0.609m, Length=0.51m

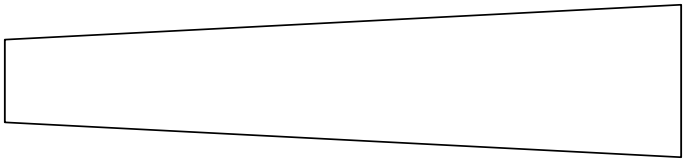

Gradual Expansion pipe: LD=0.406m, RD=0.609m, Length=1.83m

Figure 22 Different Discharge Pipe Configurations

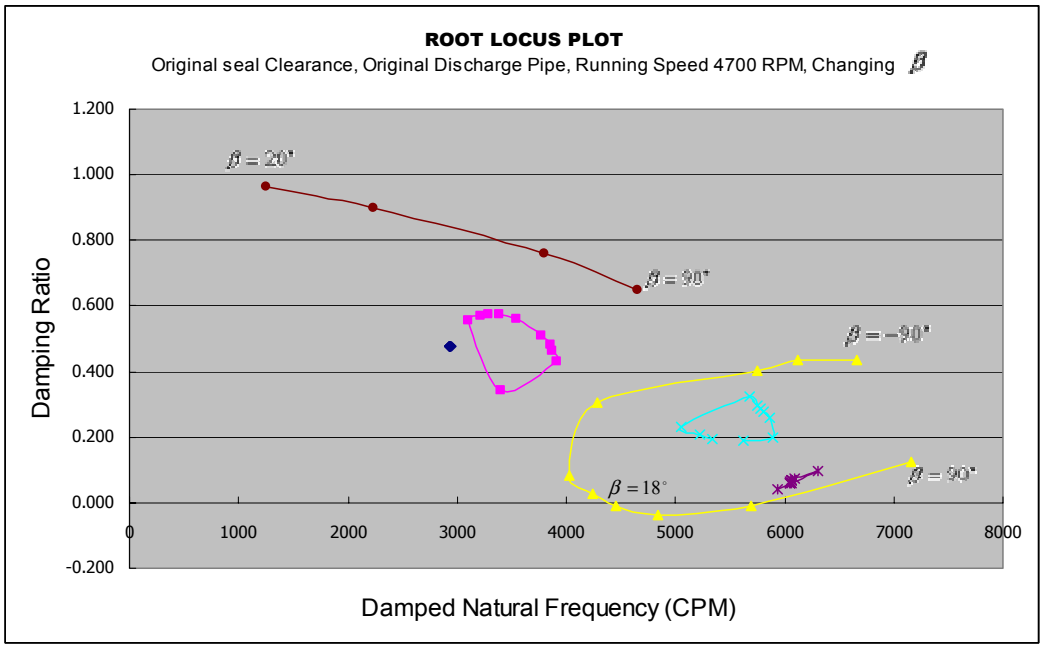

Figure 23 Rotordynamic Root Locus Plot with Original-clearance Seal and Abrupt Expansion at the Running Speed of 4700 RPM

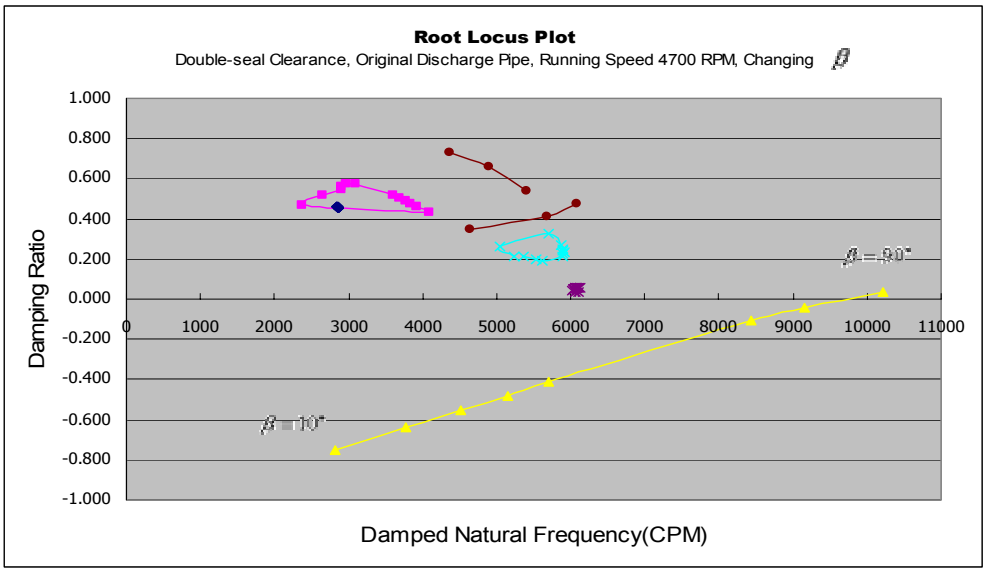

Figure 24 Rotordynamic Root Locus Plot with Double-clearance Seal and Abrupt Expansion at the Running Speed of 4700 RPM

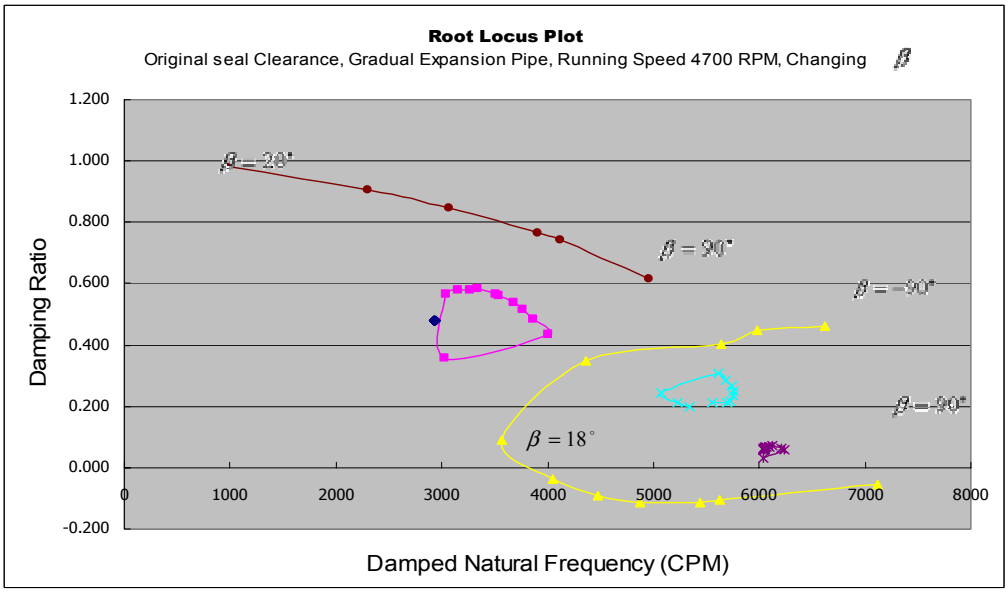

Figure 25 Rotordynamic Root Locus Plot with Original-clearance Seal and Gradual Expansion at the Running Speed of 4700 RPM

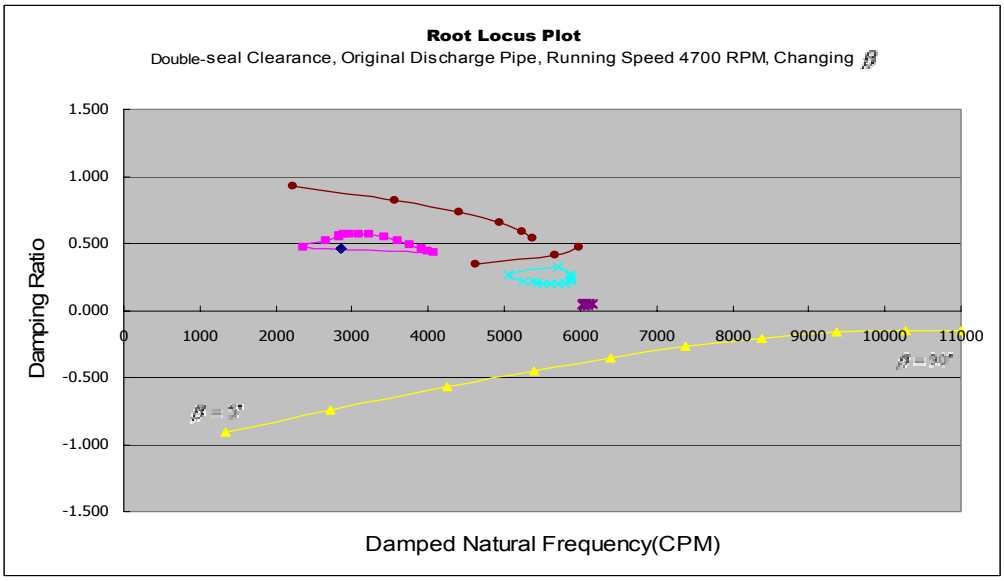

Figure 26 Rotordynamic Root Locus Plot with Double-clearance Seal and Gradual Expansion at the Running Speed of 4700 RPM

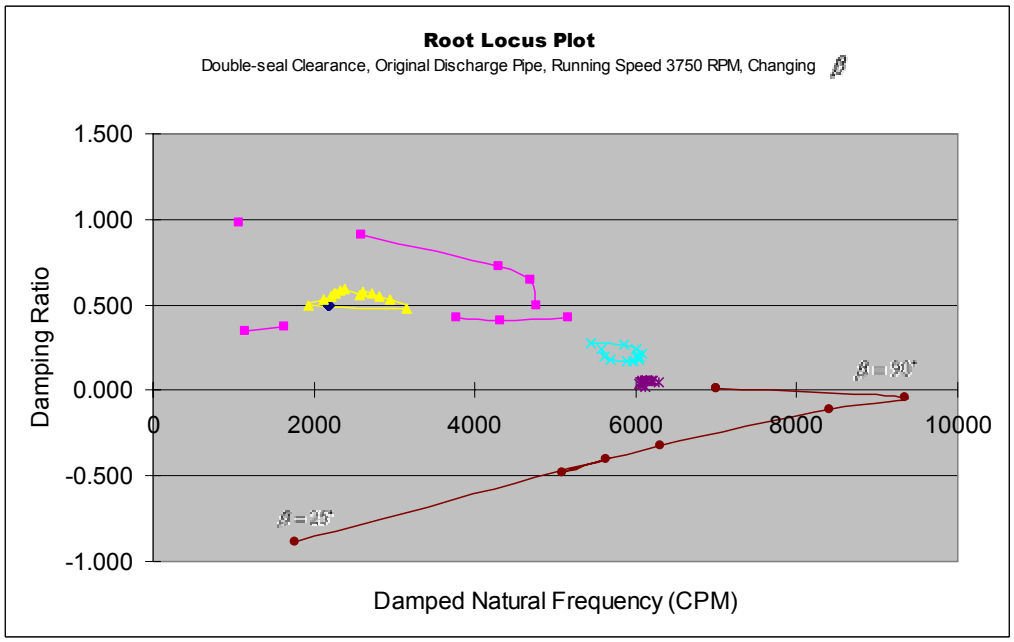

Figure 27 Rotordynamic Root Locus Plot with Original-clearance Seal and Abrupt Expansion at the Running Speed of 3750 RPM

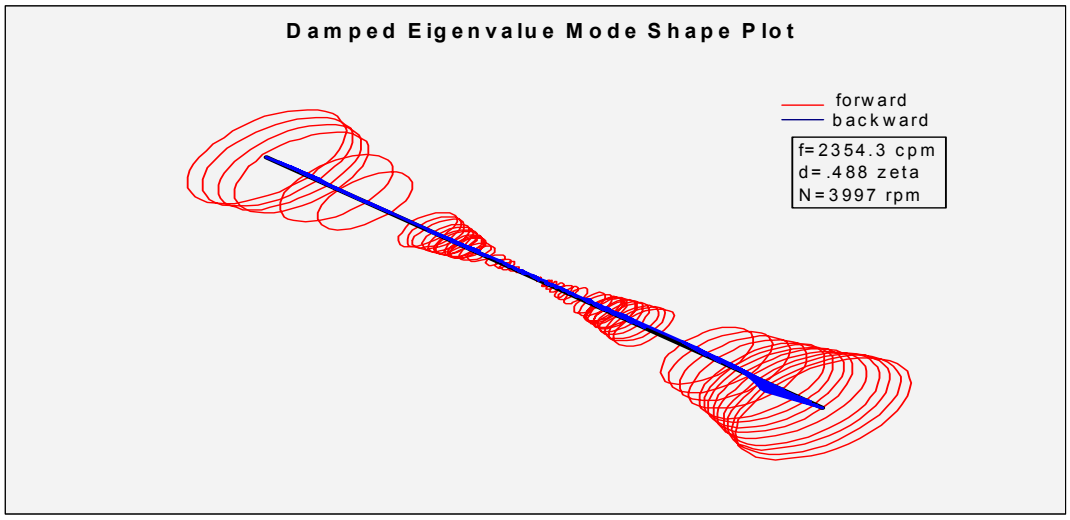

Figure 28 1st Damped Mode Shape with Water-hammer Coupling, Double-clearance Seal, $\beta = 15^{\circ}$

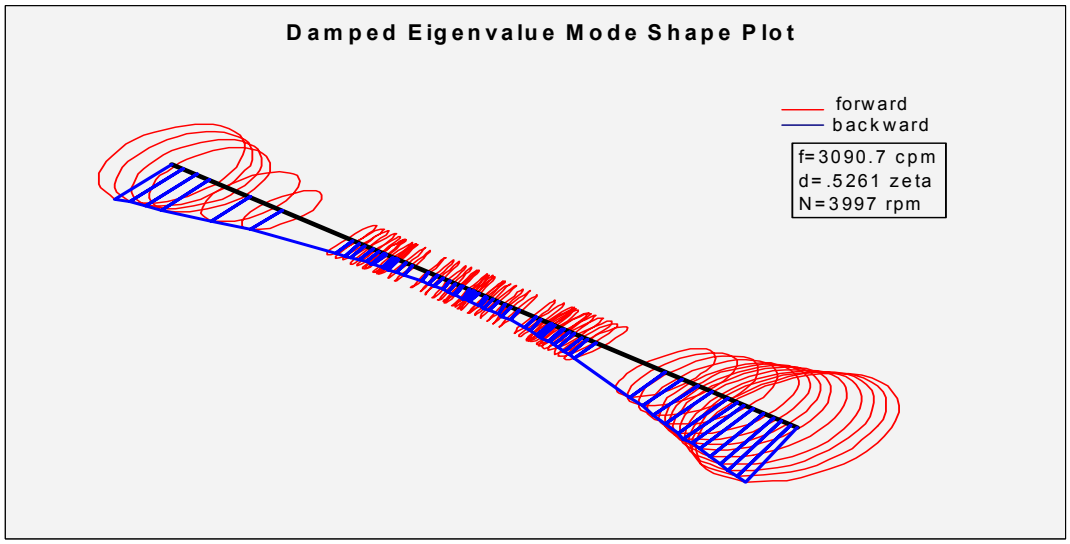

Figure 29 2nd Damped Mode Shape with Water-hammer Coupling, Double-clearance Seal, $\beta = 15^{\circ}$

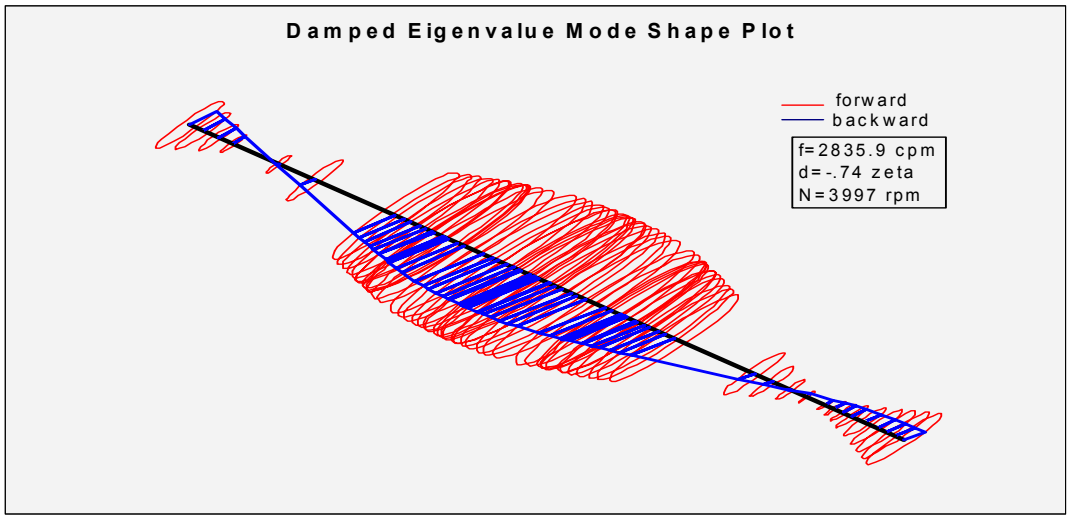

Figure 30 3rd Damped Mode Shape with Water-hammer Coupling, Double-clearance seal, $\beta = 15^{\circ}$

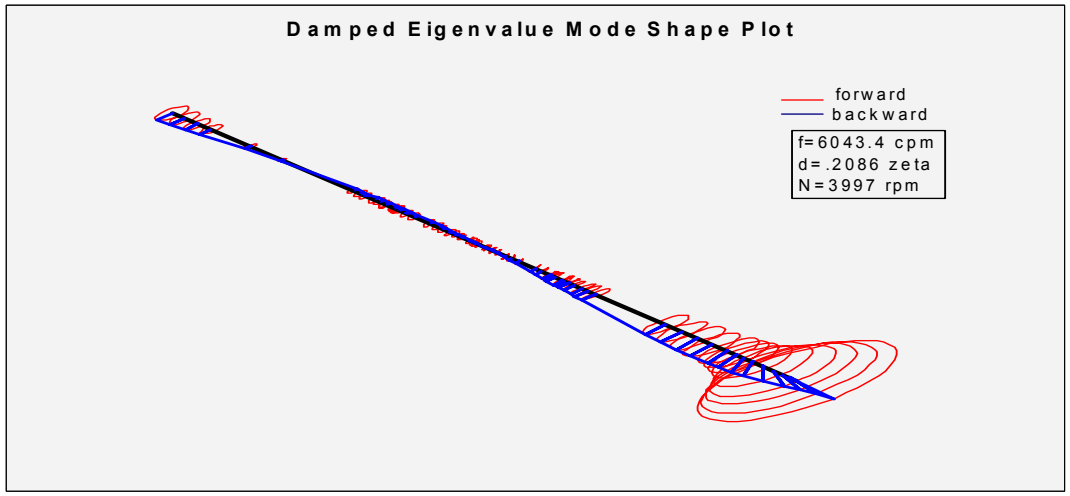

Figure 31 4th Damped Mode Shape with Water-hammer Coupling, Double-clearance Seal, $\beta = 15^{\circ}$

1. Effects of the reaction force angle β

Figure 23 to Figure 27 show the rotordynamic root locus plots where the reaction-force angle is changing (the data points with the same color have different reaction-force

angle). Figure 28 to Figure 31 show the first four damped modes with water-hammer coupling, double-seal clearances and $\beta = 15^{\circ}$. The following phenomena can be seen from these figures: 1) Two damped natural frequencies remain almost unchanged with changes to the reaction-force angle. Recalling the mode shapes given in Figure 3 to Figure 6, this result is reasonable since the seal perturbation location coincides with the vibration node. 2) The other natural frequencies are significantly shifted by the reaction force angle, either stabilized or destabilized. 3) Instabilities are predicted in certain range of angle β between 0 and 90 degrees with a sinusoidal mode shape. This range changes with different seal clearances, running speed and discharge transition configurations. There is uncertainty in the reaction force angle β, at which instability could be predicted precisely. With original-clearance seal and abrupt discharge transition at the running speed 4700 RPM, this range is about 18 to 85 degrees. With double-seal clearance and abrupt discharge transition at the running speed 4700 RPM, this range is about 10 to 90 degrees. With original-clearance seal and gradual discharge transition at the running speed 4700 RPM, this range is about 18 to 90 degrees. With double-seal clearance and gradual discharge transition at the running speed 4700 RPM, this range is about 5 to 90 degrees. Also, the instability frequency changes dramatically with the reaction force angle β, from 2000 CPM to 100000 CPM. 4) No instability is reported by computer simulation if the reaction-force angle is located in the range from -90 degrees to 0 degree.

2. Effects of seal clearances

Comparison of Figure 23 and Figure 24 shows that seal clearance has a significant effect on the rotordynamics characteristics. Besides what is mentioned before in section III.2, a double-clearance seal can enlarge the flow-rate perturbation as shown in Figure 14 to Figure 17; hence, making the problem worse. The instabilities observed in Figure 24 (with double-clearance seal) have much larger negative damping ratios than those in figure 20 (with the original-clearance seal). Also, instability appears only for the reaction force angle β ranging from 18 to 90 degrees in Figure 23, while in Figure 24, instability appears in a range of β from 5 degrees to 90 degrees. Similar results hold for Figure 25 and Figure 26.

Figure 32 and Figure 33 show the rotordynamic natural frequency map and root locus plot with original-clearance seal, original discharge transition and $\beta = 15^{\circ}$. Figure 34 and Figure 35 show the rotordynamic natural frequency map and root locus plot with the double-clearance seal, original discharge transition and $\beta = 15^{\circ}$. With the original-clearance seal, the unit is marginally stable through out the speed range. With double-clearance seals, a sub-synchronous instability component shows up with a precession frequency of 3200 RPM. The unstable frequency increases with running speed and approaches to another natural frequency, which is close to what was observed in the field.

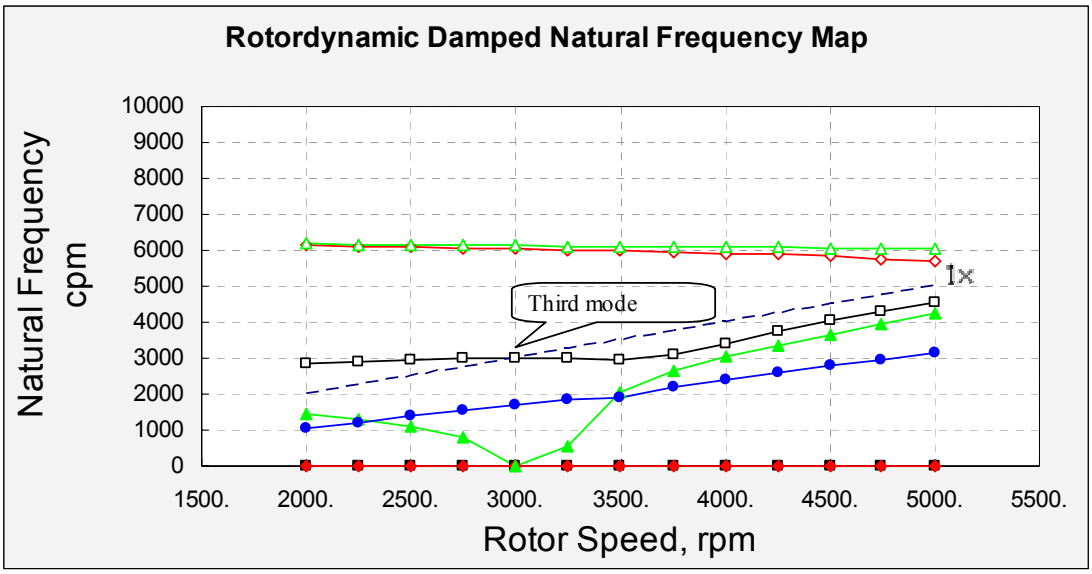

Figure 32 Rotordynamic Damped Natural Frequency Map with Original-clearance Seal, Original Discharge Transition, $\beta = 15^{\circ}$

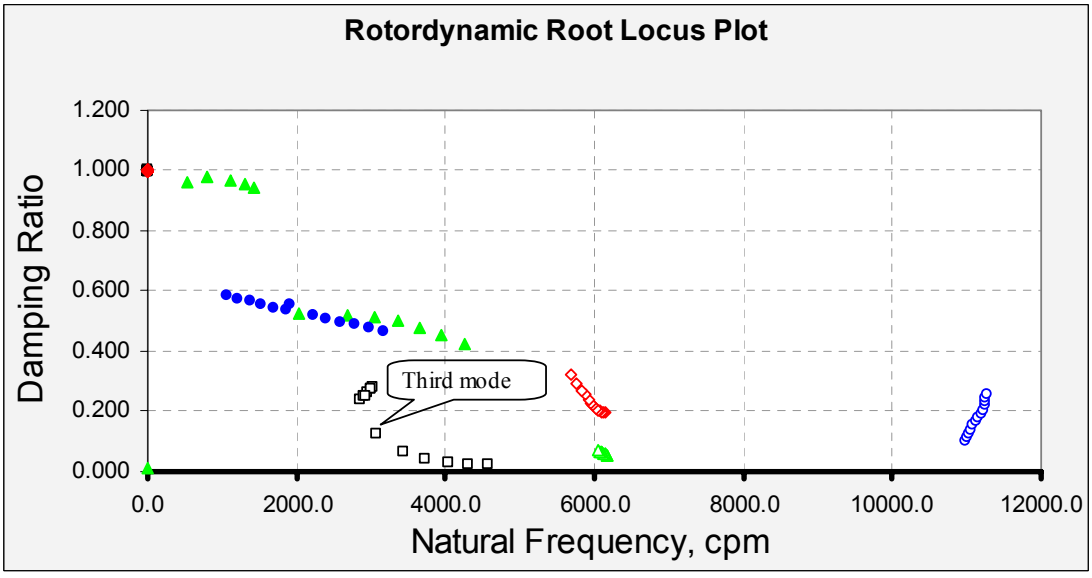

Figure 33 Rotordynamic Root Locus Plot with Original-clearance Seal, Original Discharge Transition, $\beta = 15^{\circ}$

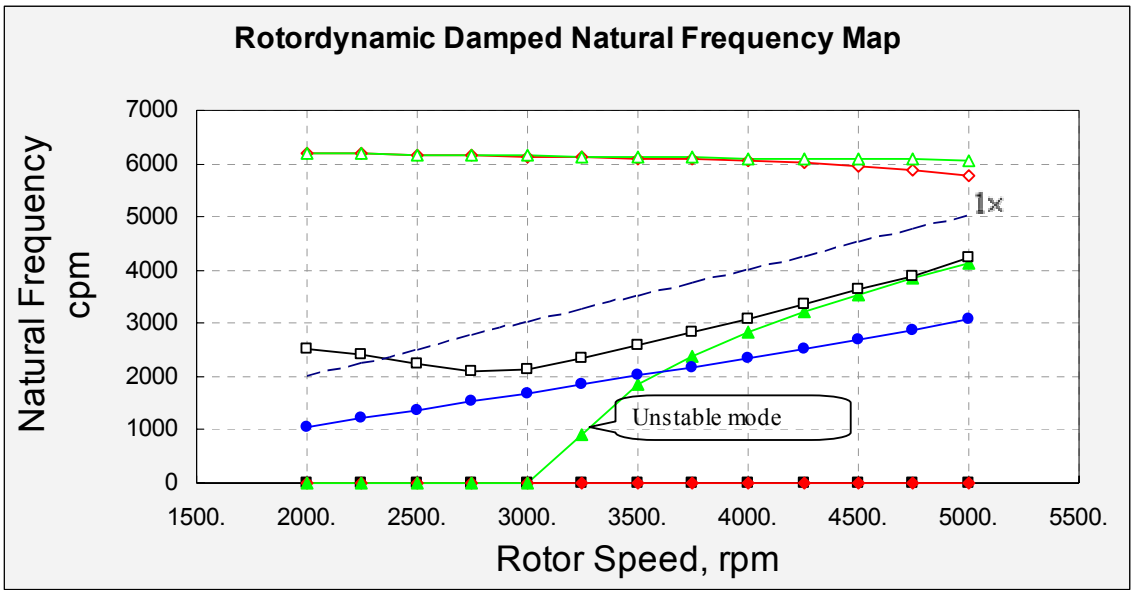

Figure 34 Rotordynamic Damped Natural Frequency Map with Double-clearance Seal, Original Discharge Transition, $\beta = 15^{\circ}$

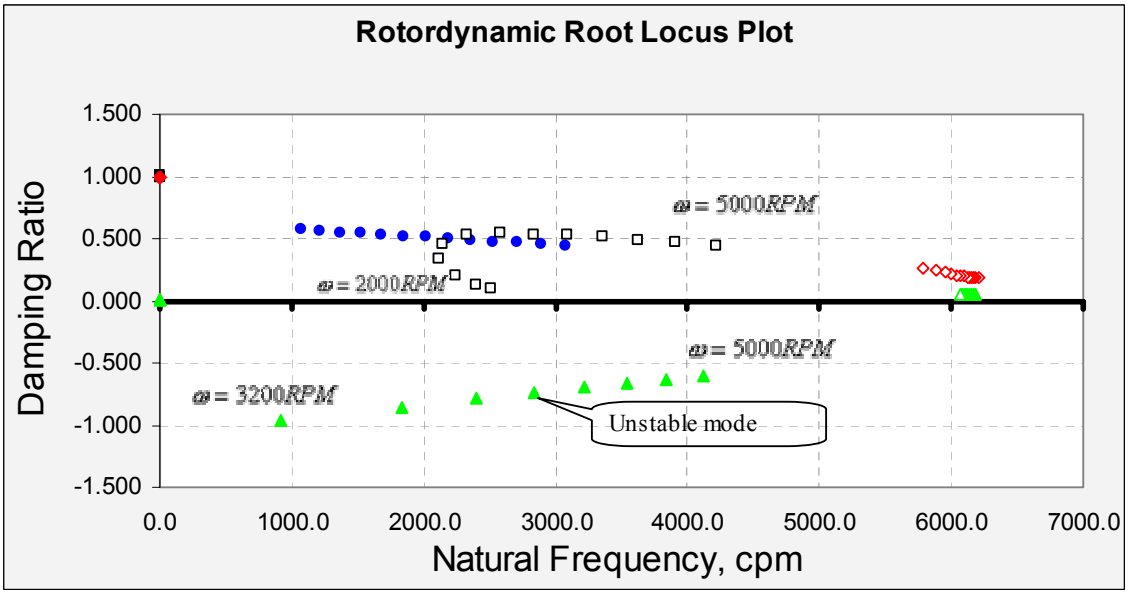

Figure 35 Rotordynamic Root Locus Plot with Double-clearance Seal, Original Discharge Transition, $\beta = 15^{\circ}$

3. Effects of discharge pipe configurations

As shown in Figure 22, the modified tapered piece has a transition from 0.406 m (16 in) to 0.609 m (24 in) over a span of 1.83 m (72 in) instead of original 0.51 m (20 in). Figure 23 and Figure 25 show the rotordynamic root locus plot with the original abrupt expansion transition and the modified gradual expansion transition respectively. Similarity is found between these two figures. An infinite termination without a tapered transition piece is also examined. Figure 36 shows the rotordynamic root locus plot with an infinite termination and double-clearance seals. Comparison with figure 6 (rotordynamic root locus plot with doubled clearance seal and without water hammer coupling) shows that the infinite termination has no visible influence on the rotordynamic characteristics.

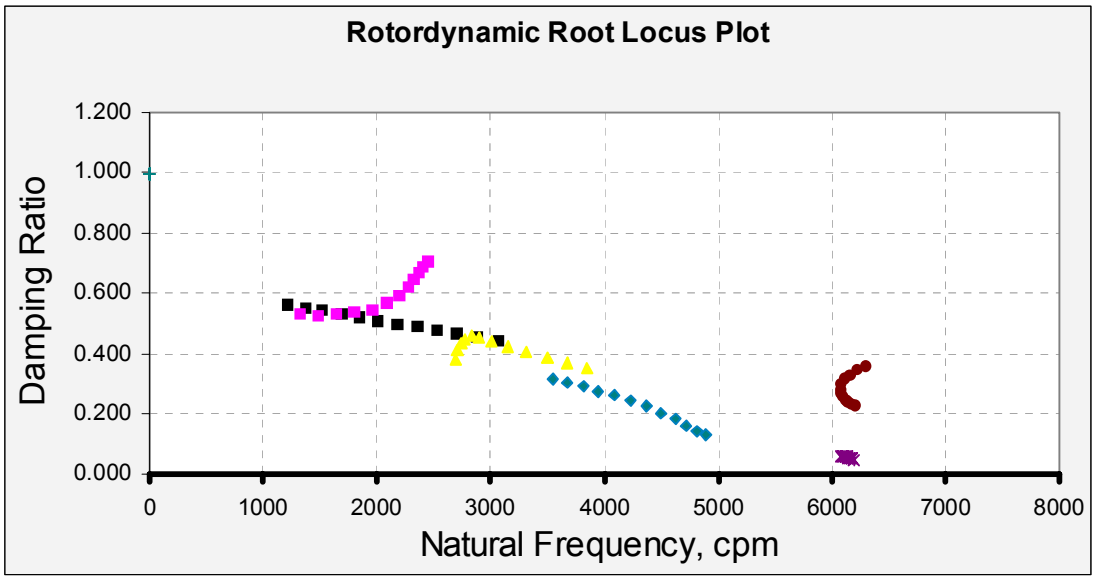

Figure 36 Rotordynamic Root Locus Plot with an Infinite Termination and Double-clearance Seal

4. Effects of running speed

Figure 24 and Figure 27 show the rotordynamic root locus plots with double-clearance seal, the original discharge transition for speeds equal to 4700 RPM and 3750 RPM, respectively. Comparison shows that rotordynamic characteristics are quite similar. Instabilities are predicted in a narrower range of angle (β) at 3750 RPM. Therefore, a lower running speed has a little better performance.

5. Comparison with field results

The field test (Corley[1]) shows that the unit with original-clearance seals has a well-damped critical at 2800 RPM. In the unstable units, at a speed of approximately 3300 RPM, a beating phenomenon appears in the vibration pattern, which means two discrete frequencies are close together. As the speed increases further, these two frequencies separate from each other. The sub-synchronous vibration component has a slight increase in frequency with increase in running speed, while the amplitude increases dramatically, which can be seen in Figure 37. After replacing the abrupt expansion discharge transition pipe with a gradual expansion transition pipe, the sub-synchronous vibration component disappeared. Figure 38 shows the horizontal shaft vibration at inboard bearing after installation of the long taper transition. Comparison of the present model results and field results shows that this model can predict a sub-synchronous instability with a double-clearance seal and the original abrupt expansion discharge pipe at $\beta = 15^{\circ}$, with a precession frequency at around 3200 RPM, as Figure 35 shows. After replacing of abrupt

discharge transition with gradual discharge transition, the new model doesn't yield the same influences on stability as field test shows, which implies that there might be some other mechanism drives this problem.

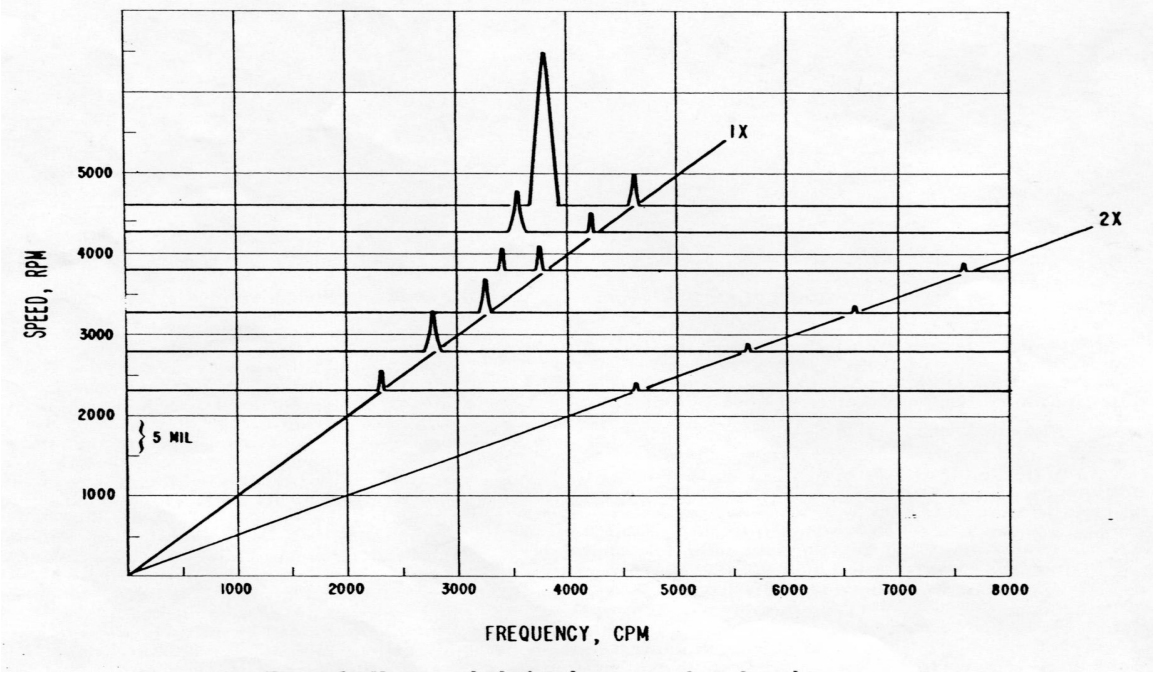

Figure 37 Horizontal Shaft Vibrations at the Inboard Bearing, Corley[1]

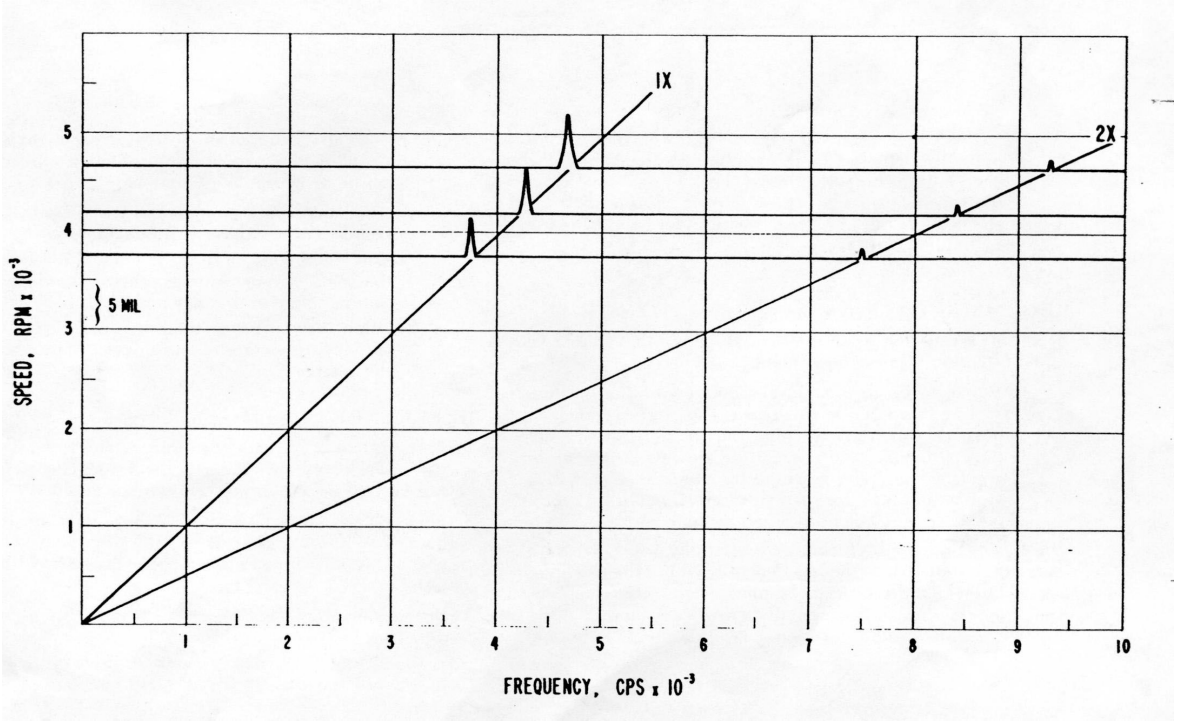

Figure 38 Horizontal Shaft Vibrations at the Inboard Bearing After Installation of Long Taper Transition, Corley [1]

VI. CONCLUSIONS

A feedback frequency-domain rotordynamics/water-hammer coupling model has been developed to simulate a field pump vibration problem. The model successfully duplicates the field results of the sub-synchronous instability. Coupling of motions at seal and the reaction force can markedly shift natural frequencies and damping. Seal clearances, reaction force angle, and discharge pipe taper-configurations can influence the rotordynamic characteristics significantly. The following conclusions are drawn from the above developments, calculations and comparisons:

1). The impeller reaction force has a significant effect on rotordynamic characteristics.

2). This water-hammer coupling model can predict sub-synchronous instability observed in the field successfully, with double-clearance seals.

3). The increase of seal clearance can reduce damping and stiffness. With water-hammer coupling, the increase of seal clearance results in greater perturbations in flow-rate, thus inducing instability.

4). The reaction-force angle significantly influences the rotordynamic characteristics. Instability component either sub-synchronous or super-synchronous may be induced for certain ranges of β . Uncertainty is found regarding the influences of β on the rotordynamic characteristics. It is yet to understand how to calculate the reaction force angle in field.

5). By varying the reaction-force angle β, similar rotordynamic characteristics are observed with abrupt and gradual discharge transition. An infinitely long termination does not influence the rotordynamic characteristics.

6). The predicted rotordynamic characteristics are similar at running speed 3750 RPM and 4700 RPM.

REFERENCES

[1] Corley, J.E., 1978, "Subsynchronous Vibration in a large Water Flood Pump", Proceedings, 7th Turbomachinery Symposium, pp.103-110.

[2] Corley, J.E., 1994, "A Pump Instability Theory Using an Acoustic Feedback Mechanism", IGTI paper 94-GT-30, presented at International Gas Turbine and Aeroengine Congress and Exposition, Den Hague, The Netherlands.

[3] Soulas, T. and San Andres, L., June 2001, "Investigation on the Relationship between the Frequency-Dependent Perturbed (First-Order) Flow-rate and the Seal Eccentricity", private communation.

[4] Dara W. Childs, 1993, "Turbomachinery Rotordynamics, Phenomena, Modeling, and Analysis", John Wiley & Sons, Inc..

[5] Y. Rocard, 1960, "General Dynamics of Vibration", Frederick UNGAR Publishing Co., New York, pp. 431-435.

[6] William T. Thomson, 1960, "Laplace Transformation", Prentice-Hall, INC., pp. 1-15.

[7] Marquette, O., 1995, "Experimental Versus Theoretical Comparison of the Static and Dynamic Characteristics of One Smooth and Two Grooved Liquid Annulas Seals with L/D of 0.457", Technical Report No. TL-SEAL-5-95, Turbomachinery Laboratory, Texas A&M University System, College Station, TX.

[8] Streeter, Victor L. and Wylie, E. B., 1967, "Hydraulic Transients", McGraw-Hill book Co., New York, pp. 102-115.

[9] George F. Kleynhans, Dara W. Childs, 1997, "The Acoustic Influence of Cell Depth on the Rotordynamic Characteristics of Smooth-Rotor/Honeycomb-Stator Annular Gas

Seals," ASME Trans., Journal of Engineering for Gas Turbines and Power, Vol. 119, No. 4, pp. 949-957.

APPENDIX A

BEARING, SEAL, IMPELLER COEFFICIENTS IN XLTRC^2

1. Pressure dam bearing rotordynamic coefficients in XLTRC^2

***XLPresDm*™ Spreadsheet for Pressure Dam Bearing Dynamic Coefficients**

Title:	Predam Bearings_zkk

Bearing Diameter	6.375	**inches**
Bearing Axial Length	3.188	**inches**
Supply Pressure	0	**psi**
Discharge Pressure	0	**psi**
Cavitation Pressure	0	**psi**
Pkt or Grv Axial Nodes	10	**--**
Land Axial Nodes	10	**--**

Selected Lubricant		
ISO 100		
Lube Film Temperature	158	**Deg F**
Viscosity at Tfilm	28.11	**cp**
Density at Tfilm	52.39	**lb/ft^3**

Pad Number --	Pad Lead Edge degrees	Pad Arc Len degrees	Preload Angle degrees	Machined Clearance inches	Preload --	Dam/Grv Arc Length degrees	Dam/Grv Axial Length inches	Dam/Grv Depth inches	Pkt/Grv Circ Nodes --	Land Circ Nodes --
1	-170	160	90	0.0048	0	125	1.594	0.024	20	10
2	10	160	90	0.0048	0	120	1.255	0.015	20	10

X Load lb	Y Load lb	Speed rpm	Kxx lb/in	Kxy lb/in	Kyx lb/in	Kyy lb/in	Cxx lb-s/in	Cxy lb-s/in	Cyx lb-s/in	Cyy lb-s/in
0	-1300	3000	1.84E+05	2.04E+05	-4.97E+05	4.86E+05	1.66E+03	-9.97E+02	-1.07E+03	3.72E+03
0	-1300	3400	2.08E+05	2.19E+05	-5.65E+05	5.50E+05	1.64E+03	-9.43E+02	-9.89E+02	3.59E+03
0	-1300	3800	2.34E+05	2.36E+05	-6.34E+05	6.11E+05	1.64E+03	-9.12E+02	-9.34E+02	3.49E+03
0	-1300	4200	2.60E+05	2.51E+05	-7.01E+05	6.72E+05	1.62E+03	-8.80E+02	-8.87E+02	3.41E+03
0	-1300	4600	2.85E+05	2.60E+05	-7.68E+05	7.33E+05	1.59E+03	-8.45E+02	-8.47E+02	3.35E+03
0	-1300	5000	3.09E+05	2.69E+05	-8.34E+05	7.94E+05	1.56E+03	-8.15E+02	-8.16E+02	3.30E+03
0	-1300	5400	3.33E+05	2.79E+05	-9.01E+05	8.53E+05	1.53E+03	-7.91E+02	-7.91E+02	3.25E+03
0	-1300	5800	3.56E+05	2.90E+05	-9.66E+05	9.11E+05	1.51E+03	-7.71E+02	-7.71E+02	3.22E+03

Speed rpm	Ecc X inches	Ecc Y inches	Max P psi	Power Loss hp	Q out ft^3/sec	Keq lb/in	WFR --	Meq lb
3000	8.30E-04	-1.18E-03	313	6.45	4.55E-03	2.26E+05	0.424	4.93E+03
3400	6.60E-04	-1.03E-03	337	8.15	5.05E-03	2.55E+05	0.418	4.43E+03
3800	5.38E-04	-9.12E-04	360	10.07	5.56E-03	2.85E+05	0.416	4.02E+03
4200	4.39E-04	-8.11E-04	384	12.22	6.06E-03	3.14E+05	0.412	3.69E+03
4600	3.59E-04	-7.26E-04	409	14.62	6.59E-03	3.42E+05	0.408	3.42E+03
5000	2.94E-04	-6.52E-04	434	17.17	7.12E-03	3.69E+05	0.403	3.20E+03
5400	2.40E-04	-5.88E-04	457	19.98	7.65E-03	3.96E+05	0.4	3.00E+03
5800	1.94E-04	-5.32E-04	482	22.93	8.12E-03	4.23E+05	0.397	2.81E+03

2. Centrifugal pump impeller rotordynamic coefficients in XLTRC2

XLPImpIr™ Spreadsheet for Centrifugal Pump Impeller Rotordynamic Coefficients

Title: impeller

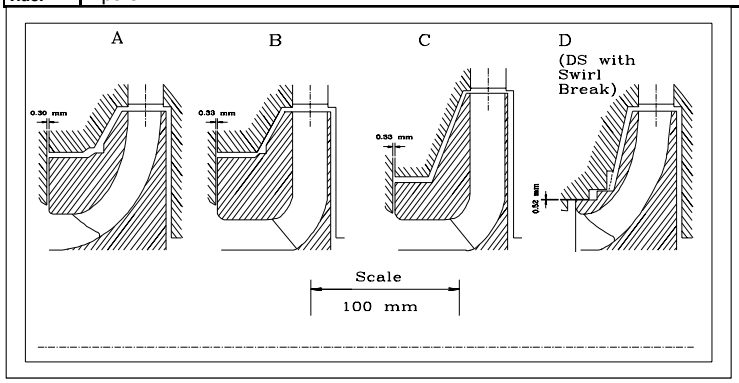

Impeller Type Choices:

A : at 2000 rpm and 30 deg C
B : at 2000 rpm and 30 deg C
C : at 2000 rpm and 30 deg. C
Da : at 2000 rpm and 60 deg. C
Db : at 4000 rpm and 60 deg. C
Dc : at 4000 rpm and 160 deg. C
Dd : at 2000 rpm and 30 deg. C

Select Impeller Type, from Table on the right and above Figure, that best describes the Geometry and Operating Conditions

Impeller Type	C	
Liquid Density	1.94	slug/ft3
Impeller Radius (r_2)	9	in
Throat Width (b_2)	2	in

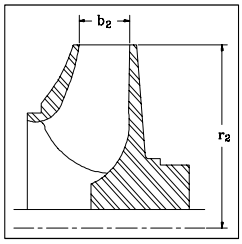

Note: Please refer to chapter 6 of the text by, Childs, D., 1993, "Turbomachinery Rotordynamics: Phenomena, Modeling, and Analysis," John Wiley & Sons Inc., for further information

Rotordynamic Coefficients

Speed	Kxx	Kxy	Kyx	Kyy	Cxx	Cxy	Cyx	Cyy	Mxx	Mxy	Myx	Myy
rpm	lb/in	lb/in	lb/in	lb/in	lb-s/in	lb-s/in	lb-s/in	lb-s/in	lb-s**2/in	lb-s**2/in	lb-s**2/in	lb-s**2/in
1	-0.00219	1.46E-03	-1.46E-03	-0.00219	0.018948	0.069807	-0.06981	0.018948	0.523762	0.095229	-0.09523	0.523762
400	-350.89	233.9265	-233.926	-350.89	7.579052	27.92282	-27.9228	7.579052	0.523762	0.095229	-0.09523	0.523762
800	-1403.56	935.7059	-935.706	-1403.56	15.1581	55.84565	-55.8456	15.1581	0.523762	0.095229	-0.09523	0.523762
1200	-3158.01	2105.338	-2105.34	-3158.01	22.73716	83.76847	-83.7685	22.73716	0.523762	0.095229	-0.09523	0.523762
1600	-5614.24	3742.824	-3742.82	-5614.24	30.31621	111.6913	-111.691	30.31621	0.523762	0.095229	-0.09523	0.523762
2000	-8772.24	5848.162	-5848.16	-8772.24	37.89526	139.6141	-139.614	37.89526	0.523762	0.095229	-0.09523	0.523762
2400	-12632	8421.353	-8421.35	-12632	45.47431	167.5369	-167.537	45.47431	0.523762	0.095229	-0.09523	0.523762
2800	-17193.6	11462.4	-11462.4	-17193.6	53.05337	195.4598	-195.46	53.05337	0.523762	0.095229	-0.09523	0.523762
3200	-22456.9	14971.29	-14971.3	-22456.9	60.63242	223.3826	-223.383	60.63242	0.523762	0.095229	-0.09523	0.523762
3600	-28422.1	18948.05	-18948	-28422.1	68.21147	251.3054	-251.305	68.21147	0.523762	0.095229	-0.09523	0.523762
4000	-35089	23392.65	-23392.6	-35089	75.79052	279.2282	-279.228	75.79052	0.523762	0.095229	-0.09523	0.523762
4400	-42457.7	28305.1	-28305.1	-42457.7	83.36958	307.1511	-307.151	83.36958	0.523762	0.095229	-0.09523	0.523762
4800	-50528.1	33685.41	-33685.4	-50528.1	90.94863	335.0739	-335.074	90.94863	0.523762	0.095229	-0.09523	0.523762
5200	-59300.4	39533.58	-39533.6	-59300.4	98.52768	362.9967	-362.997	98.52768	0.523762	0.095229	-0.09523	0.523762
5600	-68774.4	45849.59	-45849.6	-68774.4	106.1067	390.9195	-390.92	106.1067	0.523762	0.095229	-0.09523	0.523762
6000	-78950.2	52633.46	-52633.5	-78950.2	113.6858	418.8424	-418.842	113.6858	0.523762	0.095229	-0.09523	0.523762

3. Annular seal rotordynamic coefficients in XLTRC2

XLAnSeal™ Spreadsheet for Annular Seals Dynamic Coefficients
Version 2.0, Copyright 1998-1999 by Texas A&M University. All rights reserved.

Title: Annular Test Seal_zkk

Seal Diameter	12.375	inches
Seal Axial Length	2.5	inches
Inlet Radial Clearance	0.05	inches
Exit Radial Clearance	0.05	inches
Preload	0	inches
Number of Lobes	3	--
Lead Edge Location	0	degrees
Entrance Loss Coef	0.2	--
Exit Seal Coef	0	--
Supply Temperature	129	^{0}F

Selected Lubricant: Water (internal values)

Viscosity at Tsupply	48.84	cp
Density at Tsupply	53.00	lb/ft^3
Compressibility	3.15E-06	in^2/lb
Specific Heat	0.47653	BTU/(lb^{0}F)
Thermal Conductivity	0.07508	BTU/(ft-hr^{0}F)
Coef Therm Exp	0.00042	1/^{0}F
Temp Visc Coef	0.01865	1/^{0}F

Max Iterations	199	--
Momentum Relaxation Factor	0.9	--
Pressure Relaxation Factor	0.6	--
Temperature Relaxation Facto	0.9	--
Rotor Relative Roughness	0.005	--
Stator Relative Roughness	0.01	--
Moody's Coef Amod	0.001375	--
Moody's Coef Bmod	500000	--
Moody's Coef Expo	0.33333	--
No. Circ. Grid Points	21	--
No. Axial Grid Points	6	--
Inlet Swirl Ratio	0.75	--
X Static Eccentricity	0	--
Y Static Eccentricity	0	--
Moment Coef Option	Do Not Compute	
Frequency Analysis Option	Synchronous Analysis	
Constant Shaft Rpm	1000	rpm
Static Rotation About X	0	radians
Static Rotation About Y	0	radians
Seal Pivot Location	0	inches

XLAnSeal™ Spreadsheet for Annular Seals Dynamic Coefficients
Version 2.0, Copyright 1998-1999 by Texas A&M University. All rights reserved.

Title: Annular Test Seal2_zkk

Seal Diameter	9.5	inches
Seal Axial Length	2.75	inches
Inlet Radial Clearance	0.05	inches
Exit Radial Clearance	0.05	inches
Preload	0	inches
Number of Lobes	3	--
Lead Edge Location	0	degrees
Entrance Loss Coef	0.2	--
Exit Seal Coef	0	--
Supply Temperature	129	^{0}F

Selected Lubricant: Water (internal values)

Viscosity at Tsupply	48.84	cp
Density at Tsupply	53.00	lb/ft^3
Compressibility	3.15E-06	in^2/lb
Specific Heat	0.47653	BTU/(lb^{0}F)
Thermal Conductivity	0.07508	BTU/(ft-hr^{0}F)
Coef Therm Exp	0.00042	1/^{0}F
Temp Visc Coef	0.01865	1/^{0}F

Max Iterations	199	--
Momentum Relaxation Factor	0.9	--
Pressure Relaxation Factor	0.6	--
Temperature Relaxation Facto	0.9	--
Rotor Relative Roughness	0.005	--
Stator Relative Roughness	0.01	--
Moody's Coef Amod	0.001375	--
Moody's Coef Bmod	500000	--
Moody's Coef Expo	0.33333	--
No. Circ. Grid Points	21	--
No. Axial Grid Points	6	--
Inlet Swirl Ratio	0.5	--
X Static Eccentricity	0	--
Y Static Eccentricity	0	--
Moment Coef Option	Do Not Compute	
Frequency Analysis Option	Synchronous Analysis	
Constant Shaft Rpm	1000	rpm
Static Rotation About X	0	radians
Static Rotation About Y	0	radians
Seal Pivot Location	0	inches

APPENDIX B

FINITE ELEMENT MODEL DEVELOPMENT

1. Wave equations and shape functions

Y. Rocard [5] gives the wave equations governing the propagation of plane waves in horns, which can be used here to account for the expansions or contractions in the discharge lines or inlet lines.

$$c^2\left[\frac{\partial^2 u}{\partial z^2}+\frac{2}{z}\frac{\partial u}{\partial z}-2\frac{u}{z}\right]=\frac{\partial^2 u}{\partial t^2} \tag{B1}$$

$$c^2\left[\frac{\partial^2 P}{\partial z^2}+\frac{2}{z}\frac{\partial P}{\partial z}\right]=\frac{\partial^2 P}{\partial t^2} \tag{B2}$$

where u is velocity of the fluid along the pipe, P is the pressure, and c is the acoustic velocity of the pressure wave. For discharge line, pressure should be taken as dependent variable, hence, equation (B2) is considered. The weak form of equation (B2) is:

$$\begin{aligned}&\int_{z_1}^{z_2}(\rho\cdot\pi\cdot tg^2\alpha\cdot\delta P\cdot z^2\frac{\partial^2 P}{\partial t^2}+c^2\rho\cdot\pi\cdot tg^2\alpha\cdot z^2\cdot\frac{\partial(\delta P)}{\partial z}\cdot\frac{\partial P}{\partial z})dz\\&=-c^2\rho\cdot\pi\cdot tg^2\alpha\cdot\delta P\cdot {z_1}^2\frac{\partial P}{\partial z}(z_1)+c^2\cdot\rho\cdot\pi\cdot tg^2\alpha\cdot\delta P\cdot {z_2}^2\frac{\partial P}{\partial z}(z_2)\end{aligned} \tag{B3}$$

Taking one-dimensional two-node tapered element and using the static solution of the wave equation as the shape function:

$$P(z,t) = \phi_1(z)P_1(t) + \phi_2(z)P_2(t) \tag{B4}$$

$$\begin{aligned} \phi_1(z) &= \frac{-z_1 z + z_1 z_2}{(z_2 - z_1)z} \\ \phi_2(z) &= \frac{z_2 z - z_1 z_2}{(z_2 - z_1)z} \end{aligned} \tag{B5}$$

The mass matrix and stiffness matrix for each element can be derived from equation (B3) as:

$$\begin{aligned} M_{ij} &= \int_{z_1}^{z_2} \rho \cdot \pi \cdot tg^2\alpha \cdot z^2 \phi_i \phi_j dz \\ K_{ij} &= \int_{z_1}^{z_2} c^2 \cdot \rho \cdot \pi \cdot tg^2\alpha \cdot z^2 \frac{d\phi_i}{dz}\frac{d\phi_j}{dz} dz \end{aligned} \tag{B6}$$

Substitution of equation (B5) into (B6) gives:

$$M_{11} = \frac{\rho \cdot \pi \cdot tg^2\alpha \cdot z_1^{\,2}(z_2 - z_1)}{3} \tag{B7}$$

$$M_{12} = M_{21} = \frac{\rho \cdot \pi \cdot tg^2\alpha \cdot z_1 \cdot z_2(z_2 - z_1)}{6} \tag{B8}$$

$$M_{22} = \frac{\rho \cdot \pi \cdot tg^2\alpha \cdot z_2^{\,2}(z_2 - z_1)}{3} \tag{B9}$$

$$K_{11} = \frac{-c^2 \cdot \rho \cdot \pi \cdot tg^2\alpha \cdot z_1 \cdot z_2}{z_1 - z_2} \tag{B10}$$

$$K_{12} = K_{21} = \frac{c^2 \cdot \rho \cdot \pi \cdot tg^2\alpha \cdot z_1 \cdot z_2}{z_1 - z_2} \text{ (B11)}$$

$$K_{22} = -\frac{c^2 \cdot \rho \cdot \pi \cdot tg^2\alpha \cdot z_1 \cdot z_2}{z_1 - z_2} \text{ (B12)}$$

And the right hand of the equation would be:

$$Q = \{Q_1 \quad Q_2\}^T = \left\{-c^2\rho \cdot \pi \cdot tg^2\alpha \cdot {z_1}^2 \cdot \frac{\partial P}{\partial z}(z_1) \quad c^2\rho \cdot \pi \cdot tg^2\alpha \cdot {z_2}^2 \cdot \frac{\partial P}{\partial z}(z_2)\right\}^T \text{ (B13)}$$

Considering that:

$$\frac{\partial P}{\partial z} = -\rho\frac{\partial u}{\partial t} = -\rho \cdot A^{-1} \cdot \frac{\partial^2 q}{\partial t^2} \text{ (B14)}$$

Equation (B13) can be rewritten as:

$$Q = \{Q_1 \quad Q_2\}^T = \left\{c^2\rho^2\frac{\partial^2 q}{\partial t^2}(z_1) \quad -c^2\rho^2 \cdot \frac{\partial^2 q}{\partial t^2}(z_2)\right\}^T \text{ (B15)}$$

Notice that:

$$z_1 = \frac{r_1}{tg\alpha}, z_2 = \frac{r_2}{tg\alpha} \text{ (B16)}$$

The mass matrix, stiffness matrix and Q vector can be rewritten as:

$$M_{11} = \frac{\rho \cdot \pi \cdot r_1^{\,2} \cdot l}{3}$$
$$M_{12} = M_{21} = \frac{\rho \cdot \pi \cdot r_1 \cdot r_2 \cdot l}{3} \tag{B17}$$
$$M_{22} = \frac{\rho \cdot \pi \cdot r_2^{\,2} \cdot l}{3}$$

$$K_{11} = \frac{c^2 \cdot \rho \cdot \pi \cdot r_1 \cdot r_2}{l}$$
$$K_{12} = K_{21} = -\frac{c^2 \cdot \rho \cdot \pi \cdot r_1 \cdot r_2}{l} \tag{B18}$$
$$K_{22} = \frac{c^2 \cdot \rho \cdot \pi \cdot r_1 \cdot r_2}{l}$$

$$Q = \{Q_1 \quad Q_2\}^T = \left\{ c^2 \rho^2 \frac{\partial^2 q}{\partial t^2}(r_1) \quad -c^2 \rho^2 \cdot \frac{\partial^2 q}{\partial t^2}(r_2) \right\}^T \tag{B19}$$

Therefore, with pressure as the dependent variable, the system equations become:

$$[M]\{\ddot{P}\} + [K]\{P\} = \{Q\} \tag{B20}$$

Especially, where $\{Q\}$ has the form:

$$\{Q\} = \left\{ c^2 \rho^2 \frac{\partial^2 q}{\partial t^2}(r_1) \quad 0 \quad \ldots \quad -c^2 \rho^2 \frac{\partial^2 q}{\partial t^2}(r_{n+1}) \right\}^T \tag{B21}$$

For inlet line, the flow-rate should be taken as dependent variable, hence, equation (B1) with flow velocity as dependent variable is considered. Similarly, the weak form of equation (B1) can be written as:

$$\int_{z_1}^{z_2} \rho \cdot \pi \cdot tg^2\alpha \cdot \delta u \cdot z^2 \frac{\partial^2 u}{\partial t^2} + c^2 \rho \cdot \pi \cdot tg^2\alpha \cdot z^2 \frac{\partial \delta u}{\partial z}\frac{\partial u}{\partial z} + 2c^2 \rho \cdot \pi \cdot tg^2\alpha \cdot \delta u \cdot u))dz$$
$$= -c^2 \rho \cdot \pi \cdot tg^2\alpha \cdot {z_1}^2 \cdot \frac{\partial u}{\partial z}(z_1) + c^2 \rho \cdot \pi \cdot tg^2\alpha \cdot {z_2}^2 \cdot \frac{\partial u}{\partial z}(z_2) \quad \text{(B22)}$$

Considering that:

$$\frac{\partial u}{\partial z} = -\frac{1}{c^2 \cdot \rho}\frac{\partial P}{\partial t} - \frac{2}{z}u \quad \text{(B23)}$$

The right hand side of equation (B22) can be written as:

$$RHS = \pi \cdot tg^2\alpha \cdot {z_1}^2 \cdot \frac{\partial P}{\partial t}(z_1) + 2 \cdot c^2 \rho \cdot \pi \cdot z_1 \cdot tg^2(\alpha) \cdot u_1$$
$$- \pi \cdot tg^2\alpha \cdot {z_2}^2 \cdot \frac{\partial P}{\partial t}(z_2) - 2 \cdot c^2 \rho \cdot \pi \cdot z_2 \cdot tg^2(\alpha) \cdot u_2 \quad \text{(B24)}$$

Taking a two-noded element and using the static solution of equation (B1) as shape functions:

$$u(z,t) = \phi_1(z)u_1(t) + \phi_2(z)u_2(t) \quad \text{(B25)}$$

$$\phi_1(z) = \frac{{z_1}^2 z - \frac{{z_1}^2 {z_2}^3}{z^2}}{{z_1}^3 - {z_2}^3} \quad \text{(B26)}$$

$$\phi_2(z) = \frac{\frac{{z_1}^3 {z_2}^2}{z^2} - {z_2}^2 z}{{z_1}^3 - {z_2}^3} \quad \text{(B27)}$$

A matrix form equation can be derived from (B22) by substituting (B25), (B26), (B27) into it:

$$[M]\{\ddot{U}\}+[K]\{U\}=\{Q\} \tag{B28}$$

Where:

$$\begin{gathered} M_{ij}=\int_{z_1}^{z_2}\rho\cdot\pi\cdot tg^2\alpha\cdot z^2\phi_i\cdot\phi_j dz, K_{ij}=\int_{z_1}^{z_2}c^2\rho\cdot\pi\cdot tg^2\alpha\cdot(z^2\cdot\frac{d\phi_i}{dz}\frac{d\phi_j}{dz}+2\phi_i\phi_j)dz \\ U=\{u_1 \quad u_2\}^T, Q=\begin{Bmatrix}\pi\cdot tg^2\alpha\cdot z_1^2\cdot\dfrac{\partial P}{\partial t}(z_1) & -\pi\cdot tg^2\alpha\cdot z_2^2\cdot\dfrac{\partial P}{\partial t}(z_2)\\ +2\cdot c^2\rho\cdot\pi\cdot z_1\cdot tg^2\alpha\cdot u_1 & -2\cdot c^2\rho\cdot\pi\cdot z_2\cdot tg^2\alpha\cdot u_2\end{Bmatrix}^T \end{gathered} \tag{B29}$$

$$M_{11}=-\frac{\rho\cdot\pi\cdot tg^2\alpha\cdot {z_1}^3({z_1}^4+2z_2{z_1}^3+3{z_2}^2{z_1}^2-{z_2}^3z_1-5{z_2}^4)}{5({z_1}^2+z_2z_1+{z_2}^2)^2}$$

$$M_{12}=M_{21}=-\frac{3\rho\cdot\pi\cdot tg^2\alpha\cdot {z_1}^2\cdot {z_2}^2({z_1}^3+2z_2{z_1}^2-2{z_2}^2z_1-{z_2}^3)}{10({z_1}^2+z_2z_1+{z_2}^2)^2}$$

$$M_{22}=-\frac{\rho\cdot\pi\cdot tg^2\alpha\cdot {z_2}^3(5{z_1}^4+z_2{z_1}^3-3{z_2}^2{z_1}^2-2{z_2}^3z_1-{z_2}^4)}{5({z_1}^2+z_2z_1+{z_2}^2)^2}$$

$$K_{11}=\frac{-c^2\cdot\rho\cdot\pi\cdot tg^2\alpha\cdot z_1\cdot({z_1}^3+2{z_2}^3)}{{z_1}^3-{z_2}^3}$$

$$K_{12}=K_{21}=\frac{3c^2\rho\cdot\pi\cdot tg^2\alpha\cdot {z_1}^2\cdot {z_2}^2}{{z_1}^3-{z_2}^3}$$

$$K_{22} = \frac{-c^2 \rho \cdot \pi \cdot tg^2 \alpha \cdot z_2 (2z_1^{\,3} + z_2^{\,3})}{z_1^{\,3} - z_2^{\,3}}$$

Substituting equation (B16) into (B29), mass matrix, stiffness matrix and RHS can be written as:

$$M_{11} = \frac{\rho \cdot \pi \cdot r_1^{\,3} (r_1^{\,3} + 3r_2 \cdot r_1^{\,2} + 6r_1 r_2^{\,2} + 5r_2^{\,3}) \cdot l}{5(r_1^{\,2} + r_2 r_1 + r_2^{\,2})^2}$$

$$M_{12} = M_{21} = \frac{3\rho \cdot \pi \cdot r_1^{\,2} \cdot r_2^{\,2} (r_1^{\,2} + 3r_1 r_2 + r_2^{\,2}) \cdot l}{10(r_1^{\,2} + r_2 r_1 + r_2^{\,2})^2} \tag{B30}$$

$$M_{22} = \frac{\rho \cdot \pi \cdot r_2^{\,3} (5r_1^{\,3} + 6r_1^{\,2} r_2 + 3r_1 r_2^{\,2} + r_2^{\,3}) \cdot l}{5(r_1^{\,2} + r_2 r_1 + r_2^{\,2})^2}$$

$$K_{11} = \frac{c^2 \rho \cdot \pi \cdot r_1 \cdot (r_1^{\,3} + 2r_2^{\,3})}{l \cdot (r_1^{\,2} + r_1 r_2 + r_2^{\,2})}$$

$$K_{12} = K_{21} = -\frac{3c^2 \cdot \rho \cdot \pi \cdot r_1^{\,2} \cdot r_2^{\,2}}{l \cdot (r_1^{\,2} + r_1 r_2 + r_2^{\,2})} \tag{B31}$$

$$K_{22} = \frac{c^2 \rho \cdot \pi \cdot r_2 \cdot (2r_1^{\,3} + r_2^{\,3})}{l \cdot (r_1^{\,2} + r_1 r_2 + r_2^{\,2})}$$

$$Q = \begin{Bmatrix} \pi \cdot r_1^2 \cdot \dfrac{\partial P}{\partial t}(r_1) & -\pi \cdot r_2^2 \cdot \dfrac{\partial P}{\partial t}(r_2) \\ +2 \cdot c^2 \cdot \rho \cdot \pi \cdot r_1 \cdot tg(\alpha) \cdot u_1 & -2 \cdot c^2 \cdot \rho \cdot \pi \cdot r_2 \cdot tg(\alpha) \cdot u_2 \end{Bmatrix}^T$$

Notice the term $2 \cdot c^2 \cdot \rho \cdot \pi \cdot r_1 \cdot tg(\alpha) \cdot u_1$ and $2 \cdot c^2 \cdot \rho \cdot \pi \cdot r_2 \cdot tg(\alpha) \cdot u_2$ in right hand side, which can be moved to left, so that the modified stiffness and RHS become:

$$K_{11} = \frac{c^2 \rho \cdot \pi \cdot r_1 \cdot (r_1^3 + 2r_2^3)}{l \cdot (r_1^2 + r_1 r_2 + r_2^2)} - 2 \cdot c^2 \cdot \rho \cdot \pi \cdot r_1 \cdot \frac{r_2 - r_1}{l}$$

$$K_{22} = \frac{c^2 \rho \cdot \pi \cdot r_2 \cdot (2r_1^3 + r_2^3)}{l \cdot (r_1^2 + r_1 r_2 + r_2^2)} + 2 \cdot c^2 \cdot \rho \cdot \pi \cdot r_2 \cdot \frac{r_2 - r_1}{l} \tag{B32}$$

$$Q = \left\{ \pi \cdot r_1^2 \cdot \frac{\partial P}{\partial t}(r_1) \quad -\pi \cdot r_2^2 \cdot \frac{\partial P}{\partial t}(r_2) \right\}^T$$

Use flow-rate as the dependent variable instead of the flow velocity, RHS of equation (B28) becomes:

$$Q = \left\{ \pi^2 \cdot r_1^4 \cdot \frac{\partial P}{\partial t}(r_1) \quad -\pi^2 \cdot r_2^4 \cdot \frac{\partial P}{\partial t}(r_2) \right\}^T \tag{B33}$$

Therefore, with flow-rate $\dot{q}$ as the dependent variable, the system equations become:

$$[M]\{\ddot{U}\} + [K]\{U\} = \{Q\} \tag{B34}$$

Especially, where $\{Q\}$ has the form:

$$\{Q\} = \left\{ \pi^2 \cdot r_1^4 \cdot \frac{\partial P}{\partial t}(r_1) \quad 0 \quad \ldots \quad 0 \quad -\pi^2 \cdot r_2^4 \cdot \frac{\partial P}{\partial t}(r_2) \right\}^T \tag{B35}$$

The acoustic velocity in a homogeneous, little compressible liquid and a rigid conduit is identical with that of sound in the liquid. Due to the elasticity of the pipe-line, the wave velocity in a conduit is less than that of sound and actually becomes a function of pipe diameter. For thin-walled pipe-lines of circular cross-section, the actual velocity may be found from the relation:

$$c = \sqrt{\frac{1}{\rho(\frac{1}{K} + \frac{D}{eE})}} \tag{B36}$$

2. Transfer function of discharge line

The equation for pressure is used for discharge line. The system equations have been given as (B20):

$$[M]\{\ddot{P}\} + [K]\{P\} = \{Q\}$$

The mass matrix and stiffness matrix are $(n+1)\times(n+1)$ square matrices, provided that n elements were taken for the discharge pipe. The natural frequencies and modes can be obtained by solving the general eigenvalue problem:

$$-\omega^2 M\lambda = K\lambda \tag{B37}$$

Denote the eigenvalues and associated eigenvectors as:

$$\lambda_i, \Phi_i, i = 1,2...n+1$$

Thus the natural frequencies and mode shapes are:

$$\omega_{ni} = \lambda_i^{0.5}, \Phi_i, i = 1,2...n+1$$

Let the transformation matrix Φ be:

$$\Phi = \begin{bmatrix} \Phi_1 & \Phi_2 & ... & \Phi_n & \Phi_{n+1} \end{bmatrix} \tag{B38}$$

And define the modal coordinates:

$$\{P\} = [\Phi]\{\hat{P}\} \tag{B39}$$

It is reasonable here that only the first several modes instead of all modes are included in the transformation matrix. All the procedures will hold except that the number of modal coordinates will be different. The system equation (B20) can be diagonalized in modal space as:

$$M_m \ddot{\hat{P}} + K_m \hat{P} = Q_m \tag{B40}$$

Or in matrix form:

$$\begin{bmatrix} 1 & & & \\ & 1 & & \\ & & ... & \\ & & & 1 \end{bmatrix} \begin{bmatrix} \ddot{\hat{P}}_1 \\ \ddot{\hat{P}}_2 \\ ... \\ \ddot{\hat{P}}_n \\ \ddot{\hat{P}}_{n+1} \end{bmatrix} + \begin{bmatrix} \omega_1^2 & & & & \\ & \omega_2^2 & & & \\ & & ... & & \\ & & & \omega_n^2 & \\ & & & & \omega_{n+1}^2 \end{bmatrix} \begin{bmatrix} P_1 \\ P_2 \\ ... \\ P_n \\ P_{n+1} \end{bmatrix} = \Phi' \begin{bmatrix} c^2 \rho^2 \cdot \ddot{q}_1 \\ 0 \\ ... \\ 0 \\ -c^2 \rho^2 \cdot \ddot{q}_{n+1} \end{bmatrix}$$

Where:

$$M_m = \Phi' M \Phi = I$$

$$K_m = \Phi' K \Phi = \begin{bmatrix} \omega_1^2 & & & & \\ & \omega_2^2 & & & \\ & & \dots & & \\ & & & \omega_n^2 & \\ & & & & \omega_{n+1}^2 \end{bmatrix}$$

$$Q_m = \Phi' \cdot Q$$

By taking a Laplace transformation, it can be switched to s-domain:

$$\begin{bmatrix} s^2+\omega_1^2 & & & & \\ & s^2+\omega_2^2 & & & \\ & & \dots & & \\ & & & s^2+\omega_n^2 & \\ & & & & s^2+\omega_{n+1}^2 \end{bmatrix} \begin{bmatrix} \hat{P}_1(s) \\ \hat{P}_2(s) \\ \dots \\ \hat{P}_n(s) \\ \hat{P}_{n+1}(s) \end{bmatrix} = \Phi' \begin{bmatrix} c^2\rho^2 \cdot s \cdot \dot{q}_1(s) \\ 0 \\ \dots \\ 0 \\ -c^2\rho^2 \cdot s \cdot \dot{q}_{n+1}(s) \end{bmatrix} \quad \text{(B41)}$$

Equation (B41) can be solved easily, since it is uncoupled:

$$\hat{P}_i(s) = \frac{Q_{mi}(s)}{s^2+\omega_i^2}, i = 1,2...n+1 \quad \text{(B42)}$$

Where:

$$Q_{mi}(s) = \Phi_{1i} \times (c^2 \cdot \rho^2 \cdot s \cdot \dot{q}_1(s)) + \Phi_{(n+1)i} \times (-c^2 \cdot \rho^2 \cdot s \cdot \dot{q}_{n+1}(s)), i = 1,2...n+1 \quad \text{(B43)}$$

Therefore, the physical coordinates can be solved using equation (B39):

$$P_i(s) = \sum_{j=1}^{n+1} \Phi_{ij} \cdot \hat{P}_j(s) = \sum_{j=1}^{n+1} \Phi_{ij} \cdot \frac{Q_{mi}(s)}{s^2 + \omega_j{}^2} \tag{B44}$$

Especially, $P_1(s)$ and $P_{n+1}(s)$ are:

$$P_1(s) = \alpha_1 \cdot \dot{q}_1(s) + \beta_1 \cdot \dot{q}_{n+1}(s) \tag{B45}$$

$$P_{n+1}(s) = \alpha_2 \cdot \dot{q}_1(s) + \beta_2 \cdot \dot{q}_{n+1}(s) \tag{B46}$$

Where:

$$\begin{aligned} \alpha_1 &= \sum_{j=1}^{n+1} \frac{\Phi_{1j} \cdot \Phi_{1j} \cdot c^2 \cdot \rho^2 \cdot s}{s^2 + \omega_j{}^2}, \alpha_2 = \sum_{j=1}^{n+1} \frac{\Phi_{n+1j} \cdot \Phi_{1j} \cdot c^2 \cdot \rho^2 \cdot s}{s^2 + \omega_j{}^2} \\ \beta_1 &= -\sum_{j=1}^{n+1} \frac{\Phi_{1j} \cdot \Phi_{n+1j} \cdot c^2 \cdot \rho^2 \cdot s}{s^2 + \omega_j{}^2}, \beta_2 = -\sum_{j=1}^{n+1} \frac{\Phi_{n+1j} \cdot \Phi_{n+1j} \cdot c^2 \cdot \rho^2 \cdot s}{s^2 + \omega_j{}^2} \end{aligned} \tag{B47}$$

If the discharge line is close in the right end, then $\dot{q}_{n+1}(s) = 0$, therefore the transfer function between $P_1(s)$ and $\dot{q}_1(s)$ can be found to be $\alpha_1(s)$ as defined in equations (B47). If the discharge line is open in the right end, then $P_{n+1}(s) = 0$, the last equation of the system equations (B20) can be removed. Going through the same procedures described above, the transfer function between $P_1(s)$ and $\dot{q}_1(s)$ can be found to be $\alpha_1(s)$ as defined in equations (B47). Notice that these two cases have different natural frequencies and modes, thus the result is totally different, although the expressions are the same as:

$$G_1(s) = \frac{P_1(s)}{\dot{q}_1(s)} = \alpha_1(s) \tag{B48}$$

The most often case of boundary conditions are with resistance $\overline{R}_d$ over the right end.

$$P_{n+1}(s) = \overline{R}_d \cdot \dot{q}_{n+1}(s) \tag{B49}$$

Together with equation (B44) and (B45), the transfer function with resistance can be solved as:

$$G_1(s) = \frac{P_1(s)}{\dot{q}_1(s)} = \frac{\alpha_1 \cdot \overline{R}_d - \alpha_1 \cdot \beta_2 + \beta_1 \cdot \alpha_2}{\overline{R}_d - \beta_2} \tag{B50}$$

In this project, the discharge has miles long constant pipe. Infinite termination impedance according to Streeter and Wylie [8] can be used to model this configuration.

$$Z_C = (\frac{R + s \cdot L}{s \cdot C})^{0.5} \tag{B51}$$

Where:

$$R = \frac{8 f_m \rho}{\pi^2 \cdot D^5} \bar{q}, L = \frac{\rho}{A}, C = \frac{A}{\rho \cdot c^2} \tag{B52}$$

$f_m = 4 \cdot a_1 \left[1 + (\frac{b_2 e}{D} + \frac{b_3}{N_R})^{1/3} \right], N_R = \frac{VD\rho}{\mu}$ are Moody's friction factor and Reynold's number respectively. The input dates for infinite termination impedance are:

Mean flow-rate: $\bar{\dot{q}} = 1.2618 m^3 / \sec$

Fluid density: $\rho = 986 kg / m^3$

Fluid Viscosity: $\mu = 0.001 Pa \cdot \sec$

Pipe Diameter: $D = 0.609 m$

Flow velocity: $V = 4.33974 m / \sec$

Acoustic velocity: $c = 1280 m / \sec$

$e / D = 0.001, a_1 = 1.38E-3, b_2 = 2.0E4, b_3 = 1.0E+6$

Reynold's Number: $N_R = 2602438.581$

Moody's friction factor: $f_m = 0.020522$

Resistance: $R = 247.3136 kg / m^5 / \sec$

Capacitance: $C = 1.80222E-10 m^3 \sec^2 / kg$

Inertia: $L = 3386.66838 kg / m^5$

The calculation shows that the real part of the impedance is almost constant, while the imaginary part of the impedance looks as the following Figure B 1. Therefore, the impedance can be expressed as:

$$Z_C(s) = K_W + \frac{C_W}{s} \tag{B53}$$

In this case, $K_W = 4994935$, $C_W = 158280$.

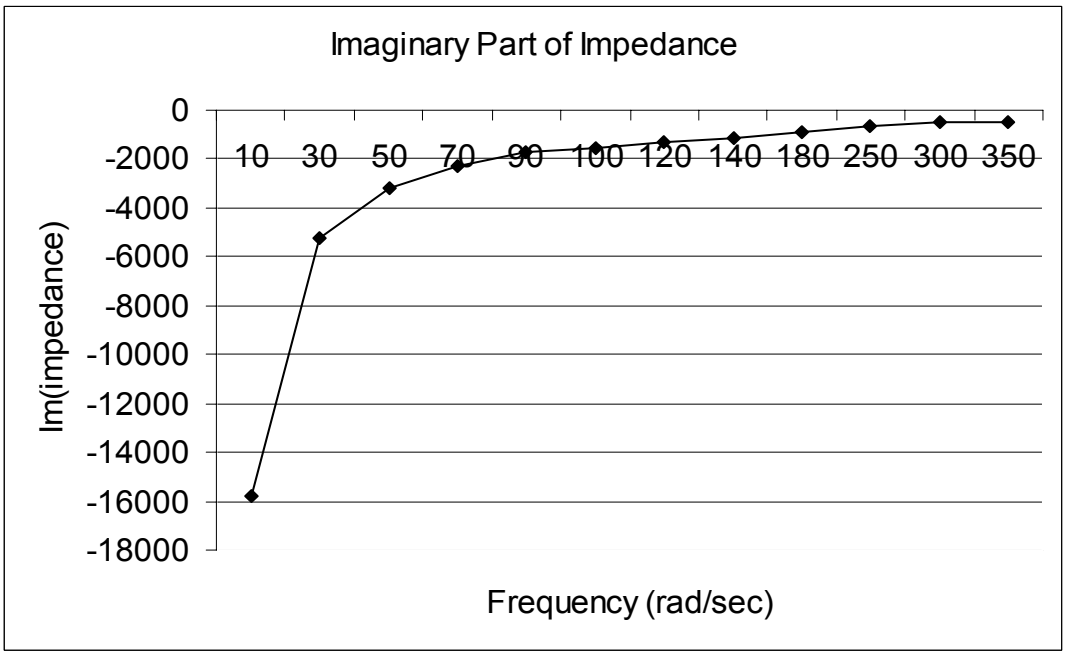

Figure B 1 Imaginary Part of Infinite Termination Impedance

3. Transfer function of inlet line

The wave equation with flow-rate as variable is used for the inlet line. The system equation has been given above as equation (B34).

$$[M]\{\ddot{U}\}+[K]\{U\}=\{Q\}$$

Similar procedures can be conducted to obtain the transfer function. The natural frequencies and modes can be obtained by solving the general eigenvalue problem:

$$-\omega^2 M\lambda = K\lambda$$

Denote the eigenvalues and associated eigenvectors as:

$$\lambda_i, \Phi_i, i = 1,2...n+1$$

Thus the natural frequencies and mode shapes are

$$\omega_{ni} = \lambda_i^{0.5}, \Phi_i, i = 1,2...n+1$$

Let the transformation matrix Φ be:

$$\Phi = \begin{bmatrix} \Phi_1 & \Phi_2 & \dots & \Phi_n & \Phi_{n+1} \end{bmatrix} \quad \text{(B54)}$$

And define the modal coordinates:

$$\{U\} = [\Phi]\{\hat{U}\} \tag{B55}$$

More often, only the first several modes are taken to reduce the computation without loosing accuracy, so that normally the modal coordinates have different dimension from physical coordinates. The uncoupled system equations in modal space are:

$$M_m \ddot{\hat{U}} + K_m \hat{U} = Q_m$$

Or in matrix form:

$$\begin{bmatrix} 1 & & & & \\ & 1 & & & \\ & & \cdots & & \\ & & & 1 & \\ & & & & 1 \end{bmatrix} \begin{bmatrix} \ddot{\hat{U}}_1 \\ \ddot{\hat{U}}_2 \\ \cdots \\ \ddot{\hat{U}}_n \\ \ddot{\hat{U}}_{n+1} \end{bmatrix} + \begin{bmatrix} \omega_1^2 & & & & \\ & \omega_2^2 & & & \\ & & \cdots & & \\ & & & \omega_n^2 & \\ & & & & \omega_{n+1}^2 \end{bmatrix} \begin{bmatrix} \hat{U}_1 \\ \hat{U}_2 \\ \cdots \\ \hat{U}_n \\ \hat{U}_{n+1} \end{bmatrix} = \Phi' \begin{bmatrix} A_1^2 \cdot \dot{P}_1 \\ 0 \\ \cdots \\ 0 \\ -A_{n+1}^2 \cdot \dot{P}_{n+1} \end{bmatrix} \tag{B56}$$

After taking a Laplace transformation, equation (B56) becomes:

$$\begin{bmatrix} s^2 + \omega_1^2 & & & & \\ & s^2 + \omega_2^2 & & & \\ & & \cdots & & \\ & & & s^2 + \omega_n^2 & \\ & & & & s^2 + \omega_{n+1}^2 \end{bmatrix} \begin{bmatrix} \hat{U}_1(s) \\ \hat{U}_2(s) \\ \cdots \\ \hat{U}_n(s) \\ \hat{U}_{n+1}(s) \end{bmatrix} = \Phi' \begin{bmatrix} A_1^2 \cdot s \cdot P_1(s) \\ 0 \\ \cdots \\ 0 \\ -A_{n+1}^2 \cdot s \cdot P_{n+1}(s) \end{bmatrix} \tag{B57}$$

Equation (B57) can be solved quickly since it is uncoupled.

$$\hat{U}_i(s) = \frac{Q_{mi}(s)}{s^2 + \omega_i^2}, i = 1,2...n+1 \tag{B58}$$

Where:

$$Q_{mi}(s) = \Phi_{1i} \times (A_1^{\,2} \cdot s \cdot P_1(s)) + \Phi_{(n+1)i} \times (-A_{n+1}^{\,2} \cdot s \cdot P_{n+1}(s)), i = 1,2...n+1 \quad \text{(B59)}$$

Given the modal space solution, the physical space solution can be obtained via equation (B55).

$$U_i(s) = \sum_{j=1}^{n+1} \Phi_{ij} \cdot \hat{U}_j(s) = \sum_{j=1}^{n+1} \Phi_{ij} \left(\frac{\Phi_{1j} \cdot A_1^{\,2} \cdot s \cdot P_1(s) - \Phi_{n+1\,j} \cdot A_{n+1}^{\,2} \cdot s \cdot P_{n+1}(s)}{s^2 + \omega_j^{\,2}}\right) \quad \text{(B60)}$$

Thus, provided that $P_{n+1}(s) = 0$, the transfer-function of inlet line is:

$$G_2(s) = \frac{U_1}{P_1} = -\sum_{j=1}^{n+1} \frac{\Phi_{1j}^{\,2} \cdot A_1^{\,2} \cdot s}{s^2 + \omega_j^{\,2}} \quad \text{(B61)}$$

4. Complete transfer function

Given equation (B50) and (B61), together with:

$$\delta \dot{q}_{discharge} = \delta \dot{q}_{pump} + \delta \dot{q}_{seal} \quad \text{(B62)}$$

$$\delta P_{inlet} = \delta P_{discharge} + \overline{A} \cdot \delta \dot{q}_{discharge} \quad \text{(B63)}$$

The complete transfer function for the pipeline can be obtained as:

$$T(s) = \frac{\delta P_{discharge}}{\delta \dot{q}_{seal}} = \frac{G_1(s)}{1 - G_1(s) \cdot G_2(s) - \overline{A} \cdot G_2(s)} \quad \text{(B64)}$$

Where $\overline{A}$ is the characteristic terminating impedance of the shipper pump calculated from the H-Q curve.

APPENDIX C

INPUT DATA FOR SEAL FLOW-RATE CALCULATION

Input data for Hseal.exe:

Rotor diameter: 0.3143 m

Film land length: 0.0635 m

Film land clearance: 0.635 mm and 1.27 mm

Dimensionless static eccentricity: 0.1 in the X direction

Supply pressure: 5.518 MPa

Discharge pressure: 0 Pa

Fluid: water

Temperature: 57 degree

Entrance loss coefficient: 0.2

Discharge loss coefficient: 0

Density: 1000 kg/m^3

Viscosity: 0.001 Pa sec

Circumferential grid points number: 41

Axial grid points number: 11

Rotor and stator relative roughness: 1E-3

APPENDIX D

EIGENVALUE CALCULATION WITH GENERAL FORM TRANSFER FUNCTIONS

A single degree freedom system is taken as an example to illustrate the procedure in detail. This single degree freedom system has mass, damping, spring characteristics m, c, k respectively. A general transfer function with numerator and denominator polynomials was incorporated. Figure D 1 shows the feedback close loop.

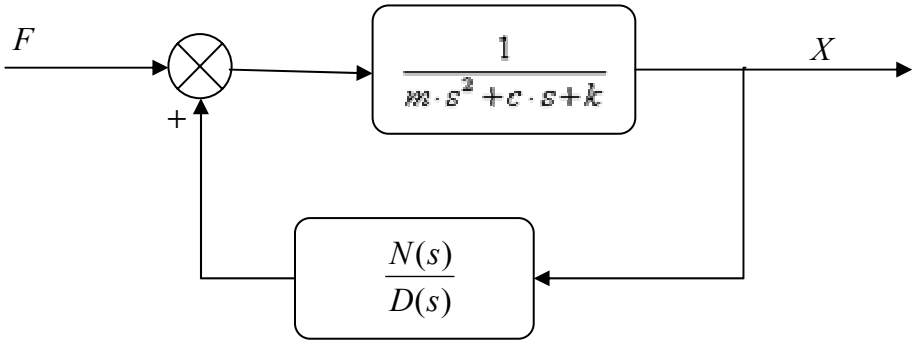

Figure D 1 Feedback close loop with general transfer function incorporated

A general form of transfer function $H(s) = \frac{N(s)}{D(s)}$ can be expanded to a form like:

$$H(s) = \frac{N(s)}{D(s)} = \sum_i \frac{A_i}{s - a_i} + \sum_i \frac{B_i s + C_i}{s^2 - c_i s + \omega_i^2} \tag{D1}$$

Therefore, equation of motion could be written as:

$$(m\cdot s^2+c\cdot s+k)X(s)+\sum_i\frac{A_i}{s-a_i}X(s)+\sum_i\frac{B_is+C_i}{s^2-c_is+\omega_i{}^2}X(s)=F(s) \tag{D2}$$

Two different types of additional terms are coming from transfer function, as we can see from equation D2. For simplicity, only consider one term for each case, in Laplace domain, by defining the new variables:

$$X_1(s)=\frac{A}{s-a}X(s)\,,\,X_2(s)=\frac{Bs+C}{s^2-es+\omega^2}X(s) \tag{D3}$$

The following model is obtained:

$$\begin{aligned}&(m\cdot s^2+c\cdot s+k)X(s)+X_1(s)+X_2(s)=F(s)\\&AX(s)-(s-a)X_1(s)=0\\&(Bs+C)X(s)-(s^2-es+\omega^2)X_2(s)=0\end{aligned} \tag{D4}$$

In time domain, the state-variable format of equation (D4) is:

$$\begin{aligned}&\dot{X}=V\\&\dot{V}=-\frac{c}{m}V-\frac{k}{m}X-\frac{1}{m}X_1-\frac{1}{m}X_2+F\\&\dot{X}_1=AX+aX_1\\&\dot{X}_2=V_2\\&\dot{V}_2=BV+CX+eV_2-\omega^2X_2\end{aligned} \tag{D5}$$

Notice that the state variable form has 5 independent states, which are 3 more than that without transfer function, one of them coming from first type, while two of them coming from second type term. Equation D5 can be stated in matrix form as:

$$[\dot{X}] = [K][X] + [F] \tag{D6}$$

The close-loop eigenvalues can be calculated directly from $[K]$.

For a single degree freedom mass, damping and spring system, the original state matrix looks like:

$$\begin{bmatrix} 0 & 1 \\ -\frac{k}{m} & -\frac{c}{m} \end{bmatrix} \tag{D7}$$

After adding rows and columns, the new state matrix looks like:

$$\begin{bmatrix} 0 & 1 & 0 & 0 & 0 \\ -\frac{k}{m} & -\frac{c}{m} & -\frac{1}{m} & -\frac{1}{m} & 0 \\ A & 0 & a & 0 & 0 \\ 0 & 0 & 0 & 0 & 1 \\ C & B & 0 & -\omega^2 & e \end{bmatrix} \tag{D8}$$

VITA

KAIKAI ZHANG

A. Personal History

Address: 6815 Rockhold Ave, San Gabriel, CA, 91775, Phone: 626-614-1901

Email Adress: mechzkk@hotmail.com

Citizenship: People's Republic of China

B. Educational History

1. Texas A&M University, College Station, Texas, 77843

Major: Mechanical Engineering

Degree: Master of Science, May 2003

2. Peking (Beijing) University, Beijing, P.R. China, 100871

Major: Mechanics

Degree: Bachelor of Science, June 2001

C. Professional Position

Graduate Research Assistant, Turbomachinery Laboratory

Texas A&M University, Part-time position, 08/2001-12/2002

D. Membership in Professional Association

American Society of Mechanical Engineers (Student Member)